

Metamorphic grade of the Madan unit in the southern part of the Central Rhodopes, Bulgaria

Emilia Raeva, Zlatka Cherneva

Abstract. The objective points of the study are orthogneisses, paragneisses and amphibolites from the Madan unit, that crop out along the Arda river valley in the southern part of the Central Rhodope and accommodate syn- to postkinematic granite bodies. The interpretation of the metamorphic grade is based on field and microstructural observations, X-ray diffraction data on K-feldspars structural state and conventional geothermobarometry. The equilibrium garnet-plagioclase-biotite assemblage of paragneisses situated in the western part of the unit define $P-T$ range of $600\text{-}670^{\circ}\text{C}/0.9\text{-}1.2$ GPa. The amphibole-plagioclase equilibrium pairs from amphibolites situated in the eastern part of the unit yield $640\text{-}720^{\circ}\text{C}/0.6\text{-}1.0$ GPa. The calculated temperatures cluster together around the water-saturated granite solidus in accordance with the field observations of initial stage of migmatization, microstructural features of amphibolite facies ductile deformation and orthoclase structure of K-feldspars in ortho- and paragneisses.

Key words: metamorphism, geothermobarometry, ductile deformation, microstructures, Madan unit, Central Rhodopes

Addresses: E. Raeva - Geological Institute, 1113 Sofia, Bulgaria; E-mail: eraeva@geology.bas.bg;
Z. Cherneva - Sofia University, 1504 Sofia, Bulgaria

Емилия Раева, Златка Чернева. Степен на метаморфизъм в Маданската единица от южната част на Централните Родопи, България

Резюме. Предмет на изследване са отрогнайси, парагнайси и амфиболити от Маданската единица, разкриващи се по долината на р. Арда в южната част на Централните Родопи и вместващи син- до посткинематични гранитни тела. Интерпретацията за степента на метаморфизъм се основава на терени и микроструктурни наблюдения, рентгено-структурни изследвания за структурното състояние на К-фелдшпати и конвенционална геотермобарометрия. Гранат-плагиоклаз-биотитовата равновесна минерална асоциация в парагнайсите, разположени в западната част на единицата, определя $600\text{-}670^{\circ}\text{C}/0.9\text{-}1.2$ GPa. Резултатите от равновесните двойки амфибол-плагиоклаз от амфиболитите, разположени в източната част на единицата, показват $640\text{-}720^{\circ}\text{C}/0.6\text{-}1.0$ GPa. Изчислени температури се групират около водонаситения гранитен солидус в съгласие с теренните наблюдения на мигматизация от метатекситов тип, с микроструктурните особености на пластична деформация в амфиболитов фациес и с ортокласовата структура на К-фелдшпати от орто- и парагнайсите.

Introduction

Modern approach to metamorphic grade evaluation requires quantitative pressure and temperature estimates, obtained from conventional thermobarometry and/or pseudosections based on combination of whole rock and mineral chemistry. The metamorphic petrology gives preferences to metapelitic and metabasitic rocks, because their mineral assemblages are more sensitive to changing metamorphic conditions and could draw the almost overall pattern of P - T metamorphic path. The quartz-feldspathic rocks and their uniform mineral assemblages, composed of feldspar, quartz, biotite \pm hornblende \pm white mica are stable at large P - T variation and cannot give complete information on the metamorphic evolution. On the other hand gneissic rocks yield abundant information on small-scale synmetamorphic deformation structures.

The most widespread rocks in the Central Rhodopes, Bulgaria are quartz-feldspar gneisses (metagranitoids predominantly). Metabasic and metasedimentary rocks although limited, crop out at different levels of the metamorphic section. Earlier estimates of metamorphic grade are based on petrographic observations of equilibrium mineral assemblages in metapelitic and metabasitic rocks mainly. Numerous studies have contributed to the conclusion of a general Barrovian style of metamorphism and transition from upper amphibolite facies accompanied by partial melting in deeper levels towards lower amphibolite to greenschist facies in the upper structural levels (Dimitrov 1955; Vergilov 1960; Vergilov et al. 1963; Kozhoukharov 1968, 1984; Kozhoukharova & Kozhoukharov 1980; Ivanov et al. 1979, 1980, 1984). The occurrence and sequential formation of Al-Si polymorphs (kyanite \rightarrow sillimanite \rightarrow andalusite) in the upper amphibolite facies section has given evidence for a general P - T path trajectory (Kostov et al. 1986) that is consistent with an orogenic geological setting.

Thermobarometric data available on the Central Rhodopes metamorphic rocks reveal decompressional P - T -path and enable suggestions about peak metamorphic conditions. Our study focuses attention on the poorly studied southernmost part that crops out along the upper course of the Arda river and straddles the Bulgarian-Greek border. The study area (Fig. 1) corresponds to the southern fragment of the Madan lithotectonic unit (Ivanov 1998; Ivanov et al. 2000; Sarov et al. 2005). A combination of results including conventional thermobarometry, microstructural indicators of synmetamorphic deformation and structural state of K-feldspar provide documentation on the metamorphic evolution of the rocks.

Geological setting

The Madan unit is a part of a metamorphic core complex in the Central Rhodopes (Fig.1) that comprises several tectonic units bounded by brittle-ductile shear zones (Ivanov et al. 2000; Sarov et al. 2004). The dome core (Arda unit) consists of high-grade amphibolite facies rocks affected by advanced melting (diatexis). The intermediate plate of the dome (Madan and Startsevo units) has undergone high-grade amphibolite facies metamorphism and initial stage of migmatization (metatexis). The non migmatic uppermost plate of the dome comprises Asenitsa unit to the north, as well as Borovitsa and Kardjali units to the east (not shown on Fig. 1) that keep record of lower amphibolite to greenschist facies metamorphism. The Madan unit crops out in two separate fragments (Fig. 1): one to the North, along the Vacha river valley; and another to the South-West, along the Arda river valley.

The orthogneisses are the most widespread rocks in the Central Rhodopean Dome. Their protoliths belong to two age groups of granitoids: late Paleozoic in the Arda unit (Arnaudov et al. 1990a; Arkadakskiy et al. 2000, 2003; Peytcheva et al. 2000, 2004; Ovtcharova et al. 2002); and late Jurassic ones

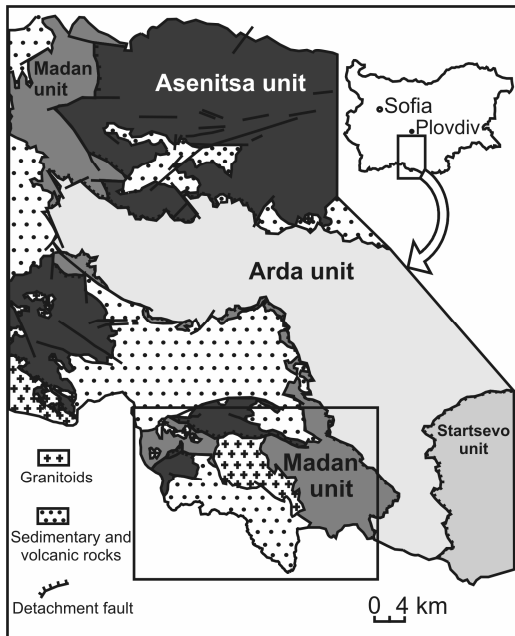


Fig. 1. Simplified geological map of the Central Rhodopean Dome (after Ivanov et al. 2000)

in the Startsevo, Borovitsa, Asenitsa, and the Madan unit fragment along the Arda river valley (Ovtcharova 2004; von Quadt et al. 2006; Raeva et al. 2008b). Metasedimentary rocks are also present in all the units in association with metabasic rocks usually. Retrogressed eclogites have been found among the latter in the Arda and Startzevo units (Kolcheva et al. 1986), Kardzhali unit (Ovtcharova et al. 2004), and in the Asenitsa unit (Ichev 1994). Limited data on the Arda unit eclogites indicate participation of Neoproterozoic oceanic crust remnants (540-610 Ma magmatic protoliths) in the Central Rhodope metamorphic complex (Arkadakskiy et al. 2003). The age of the HP metamorphic event/events is yet unknown. The moderate-pressure regional metamorphism span more than 20 Ma, from ~56 Ma to ~35 Ma, including partial melts crystallization in the migmatitic units, syn- to post kinematic granite emplacement, and sequential cooling (Arnaudov et al. 1990a, b; Arkadakskiy et al. 2000; Kaiser-Rohrmeier

2005; Ovtcharova et al. 2002, 2003; Peytcheva et al. 2000, 2004; von Quadt et al. 2006).

The decompression path of the metamorphic evolution is relatively well defined by conventional thermobarometry of metabasic and metapelitic rocks mainly. Assuming late Cretaceous to early Tertiary HP event (like in the Greek Central Rhodope, Liati 2005) one could complete the decompression path of the Arda unit based of thermobarometric results available: HT eclogite metamorphism at $780^{\circ}\text{C}/2 \text{ GPa}$ (Kolcheva et al. 1986); HP granulite facies melting during decompression in the range $700\text{-}850^{\circ}\text{C}/0.9\text{-}1.9 \text{ GPa}$ (Cherneva et al. 2008; Cherneva & Georgieva 2007; Georgieva et al. 2007); final migmatite melt crystallization at $650\text{-}700^{\circ}\text{C}/0.65\text{-}0.8 \text{ GPa}$ (Cherneva et al. 1997; Kostov et al. 1986) and subsequent decompression cooling to $550\text{-}600^{\circ}\text{C}/0.5 \text{ GPa}$ (Cherneva et al. 1997; Georgieva et al. 2002, 2007).

The Startsevo unit peak conditions of eclogite facies metamorphism are estimated as $\sim 800^{\circ}\text{C}/1.7\text{-}1.8 \text{ GPa}$, followed by granulite overprint at temperatures greater than $\sim 700^{\circ}\text{C}/\sim 1.0\text{-}1.3 \text{ GPa}$ (Carrigan et al. 2006). The corresponding estimates of Machev & Kolcheva (2008) are $730\text{-}770^{\circ}\text{C}/2.0\text{-}2.2 \text{ GPa}$ for the HP event, $850\text{-}880^{\circ}\text{C}$ at lower pressure for the granulite facies, and amphibolite facies equilibration at $655\text{-}736^{\circ}\text{C}/0.8\text{-}1.2 \text{ GPa}$. Gneisses and schists from the same unit give the range $600\text{-}660^{\circ}\text{C}/0.7\text{-}0.9 \text{ GPa}$ and a transition through $550\text{-}580^{\circ}\text{C}/0.6\text{-}0.4 \text{ GPa}$ to $440\text{-}550^{\circ}\text{C}/0.2\text{-}0.3 \text{ GPa}$ (Ovcharova 2004). The thermobarometric estimates on metabasic rocks $540\text{-}600^{\circ}\text{C}/0.6 \text{ GPa}$ (Pristavova 1995) overlap some of the above results.

The Madan unit along the Vacha river valley have had similar metamorphic evolution in the stage of amphibolite facies decompression like the Startsevo unit: from $650\text{-}670^{\circ}\text{C}/0.7\text{-}0.8 \text{ GPa}$ in the lower structural level to $625^{\circ}\text{C}/0.6\text{-}0.7 \text{ GPa}$ in the higher structural level of the tectonic unit (Cherneva et al. 1995).

The Asenitsa unit pelitic schists yield peak metamorphic conditions at $\sim 550^{\circ}\text{C}/1.35$

GPa (Guiraud et al. 1992). Data on structural state of K-feldspar (Arnaudova et al. 1990) support the results of the Asenitsa unit lower metamorphic grade. The latter study makes a general distinction based on the K-feldspar structural state: orthoclase in migmatitic units; and microcline in not affected by magmatization ones.

The study area coincides with the Madan unit that crops out along the Arda river valley (Figs. 1, 2). The dominant rocks are migmatitic biotite orthogneisses (Sarov et al. 2005; Raeva et al. 2008a) of late Jurassic protolith age (160 Ma, Raeva et al. 2008b). Mica schists, paragneisses, and marbles crop out mostly in the north-western parts of the unit, whereas amphibolites occur predominantly in the south-western parts (Katskov et al. 1962; Belmustakova 1995; Kozhoukharov et al. 1989). The metamorphic grade is supposed to correspond to upper amphibolite facies, based on common petrographic observations. Syn- to post-

kinematic granite bodies intruded the orthogneisses. A strike-slip shear zone controlled granite emplacement (Sarov et al. 2005; Naydenov et al. 2005) that happened in a short time span from 43 Ma for the synkinematic bodies to 41 Ma for the post-kinematic Smilian pluton (Ovtcharova et al. 2003; Kaiser-Rohrmeier 2004; Raeva et al. 2008b). The Madan unit continuation to the South corresponds to the so called Upper unit on the territory of Greece (Papanikolaou & Panagopoulos 1981), whose metamorphic evolution has focused attention recently with regard to UHP metamorphic relics (Schmidt et al. 2009 and references therein).

The dominant Madan unit orthogneisses have unclear foliation, massive structure, round to lens-shaped former feldspar porphyroclasts as well as elongated fine-grained melanocratic enclaves, parallel to the gneiss foliation (Raeva et al. 2008a). Evidence of *in situ* migmatization

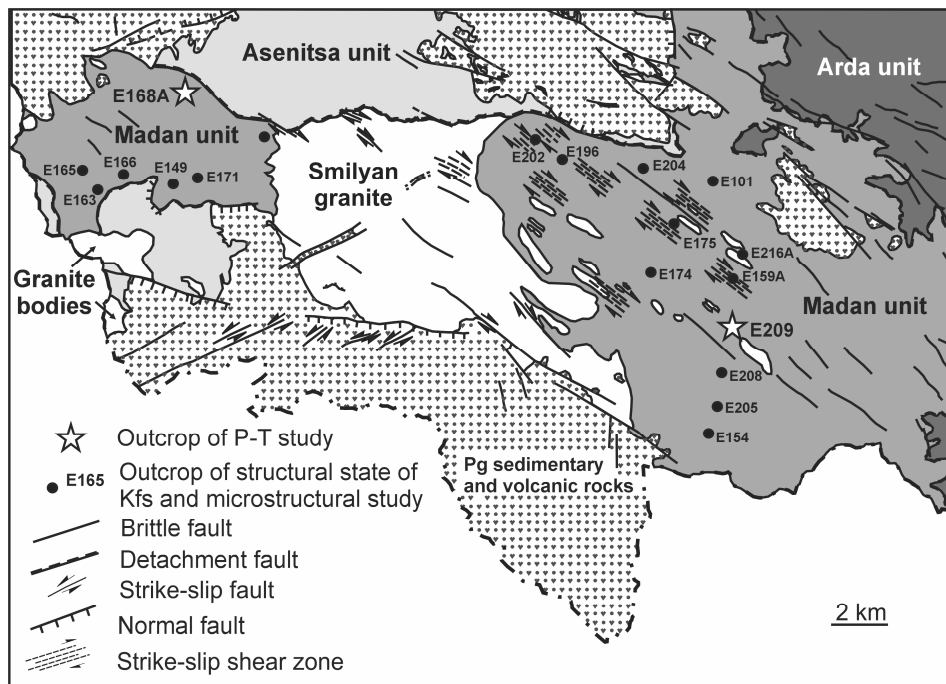


Fig. 2. Tectonic sketch map of the study area (after Sarov et al. 2005)

is present as concordant with the foliation discontinuous leucosome bands, ~3–4 mm to 1–1.5 cm thick. Ptigmatic leucosomes although rare, occur as well as leucosomes filling local ductile shear zones across the gneiss foliation.

Minor paragneisses form discontinuous bands among the orthogneisses near the Asenitsa unit marbles (Fig. 2, E168A). These are brownish-grey, fine-grained, fine-foliated, garnet- and tourmaline-bearing biotite gneisses. Thin non penetrative leucosomes occur locally in the paragneisses concordant to the gneiss foliation, completing the field features of initial stage of metatexite type of migmatization in the study area.

The metabasic rocks among the orthogneisses represent metric to tens-metric scale lens-like bodies. The amphibolites are dark-greenish, fine-grained, and clearly foliated metamorphic rocks.

Abundant granite, aplite and pegmatite veins penetrate the Madan unit rocks (Sarov et al. 2005). Pre-, and/or syn-, and postmetamorphic injections could be distinguished among the veins. The first two groups of veins are concordant to or pass across the gneiss foliation, producing small offsets along the foliation planes and diffuse contacts with migmatitic leucosomes. Their generation could be related to the gneiss protoliths or to the melt migration during migmatization. Postmetamorphic aplite and pegmatite veins have clear and sharp contacts and crosscut both the gneiss foliation and the synmetamorphic veins.

Materials and methods

Selected samples of orthogneisses, paragneisses and amphibolites from the Madan unit are studied. The orthogneiss samples (black points on Fig. 2) represent the dominant rocks to the East and to the West of the Smilyan granite. The studied paragneisses crop out in the north-western part of the Madan unit (sample E168A, N41°31'13", E24°37'37"). The amphibolite samples represent metric scaled lens-shaped body among the orthogneisses to the east of the Smilyan granite (sample E209,

N41°26'49", E24°51'17").

Popular microstructural indicators are used to characterize synmetamorphic deformation and corresponding thermal conditions of mineral recrystallization: undulose to prismatic extinction in quartz, and patchy undulose extinction in feldspars, due to subgrain formation, refer to low-temperature microstructures below ca. 600°C (Fitz Gerald & Stunitz 1993; Passchier & Trouw 1996; Kruhl 1996); 'chessboard' pattern in quartz and 'core-mantle' structures in feldspars indicate high-temperature conditions above ca. 620–650°C (Passchier & Trouw 1996; Kruhl 1996; Albertz 2006).

The structural state of K-feldspars from ortho- and paragneisses is an indicator of the cooling history of the rocks. K-feldspar fractions, obtained by routine procedure of mineral separation, have been used for X-ray diffraction analysis of the K-feldspar structural state. The structural types were determined from measurements of the $\bar{2}04$, 060 and 131 (1 $\bar{3}$ 1 resp.) reflections on powder diffractograms, following the method of the three reflections of Wright (1968). K-feldspar analyses are implemented with TUR M62 X-Ray Diffractometer at the Sofia University.

Chemical compositions of rock forming minerals in selected samples were used for thermobarometric calculations. Microprobe analyses were performed using Jeol Superprobe 733 electron microprobe at the Geological Institute of the Bulgarian Academy of Sciences and Jeol JSM-6310 electron microscope at the University of Graz, Austria, with 15 kV accelerating voltage and 100 s counting time.

The mineral abbreviations used are according to Siivola & Schmid (2007).

Petrography and microstructural relations

Orthogneisses

The major minerals are plagioclase, K-feldspar, quartz and biotite. The accessory mineral assemblage includes apatite, zircon, allanite,

titanite and magnetite and rarely garnet. The orthogneiss texture is lepidogranoblastic to granoblastic.

Biotite flakes form discontinuous foliation planes and surround feldspar grains (Fig. 3a). Biotite (<1.5-2 mm) is pleochroitic from dark brown to straw yellow. Elongated sub-parallel quartz aggregates envelop feldspar porphyroblasts (Fig. 3b). Quartz grains show undulose to prismatic extinction (Fig. 3c). A clear ‘chessboard’ pattern is developed in rare large quartz grains (Fig. 3d).

Subhedral to anhedral, rounded to lens-shaped plagioclase grains (<2-3 mm) have uniform to undulose extinction. There is subgrain formation on the periphery of some of them forming “core-mantle” textures. A wedge-shaped plagioclase twinning appears in response of deformation (Fig. 3e). Antiperthitic exsolutions of rectangular or irregular shapes occur in larger plagioclase grain cores (Fig. 3e). The exsolution clusters in the plagioclase cores suggest former normal compositional zoning of original plagioclase in the magmatic protolith. Myrmekitic plagioclase peripheries and myrmekitic plagioclase inclusions occur on the contact with K-feldspar grains (Fig. 3c) that together with antiperthites indicate subsolidus and lower temperature re-equilibration.

Large, subhedral to anhedral, round to lens-shaped K-feldspar crystals (~1-1.5 mm) display usually undulose extinction. A weak to apparent cross-hatched microcline twinning occurs in some K-feldspar grains close to subgrain and grain boundaries and along microcracks (Fig. 3c). Belmustakova (1995) has described cross-hatched microcline twinning in K-feldspars as a typical feature of the gneisses in the area. According to our observations the cross-hatched twinning is not ubiquitous and it is more frequent in the Smilyan shear zone area. This indicates causal connection between observed cross-hatched twinning in K-feldspars and intensity of ductile deformation in the gneisses.

Microstructural indicators refer to deformation at high-grade metamorphic conditions in amphibolite facies ca. 600-650°C:

rounded, subhedral to lens-shaped plagioclase crystals surrounded by fine-grained, re-crystallized quartz and biotite (Fig. 3b); ‘chessboard’ pattern in quartz (Fig. 3d); wedge-shaped plagioclase twinning (Fig. 3e); ‘core-mantle’ plagioclase textures (Fitz Gerald & Stunitz 1993; Kruhl 1996; Stipp et al. 2002). The ‘chessboard’ pattern in quartz occurs especially in gneisses from the Smilyan shear zone area. Fine-flaked white mica and/or fine-grained feldspars filling plagioclase micro-cracks and subgrain boundaries suggest initial stage of partial melting (Mehnert et al. 1973; Jurewicz & Wotson 1984; Sawyer 1999). Plagioclase cracks filled with quartz, biotite and K-feldspar (Fig. 3f) indicate former melt presence (Blumenfeld & Bouchez 1988; Bouchez et al. 1992) in consistence with field observation of initial stage of migmatization (metatexis).

Paragneisses

The major mineral assemblage includes biotite, plagioclase, K-feldspar and quartz, and minor garnet. The accessory minerals are apatite, zircon, magnetite, tourmaline, titanite and epidote. The paragneiss texture is lepidogranoblastic.

Reddish-brown elongated biotite flakes (1-1.5 mm) construct continuous foliation planes, surrounding plagioclase grains (Fig. 4a). Dynamically re-crystallized quartz grains show undulose to prismatic extinction (Fig. 4b) forming discontinuous bands parallel to the foliation.

Anhedral to subhedral, rounded to lens-shaped plagioclase grains (<1 mm) are arranged also parallelly to the common foliation (Fig. 4c, d). Rare larger subhedral plagioclase grains (~1-1.5 mm) display patchy undulose extinction in response to subgrain formation. “Core-mantle” textures occur when subgrains are developed on large plagioclase grain peripheries (Fig. 4c). Some plagioclase grains show wedge-shaped twinning (Fig. 4e).

Minor amount of K-feldspar (<0.5 mm) take place in pressure shadows of plagioclase grains (Fig. 4d). Rare larger K-feldspar grains

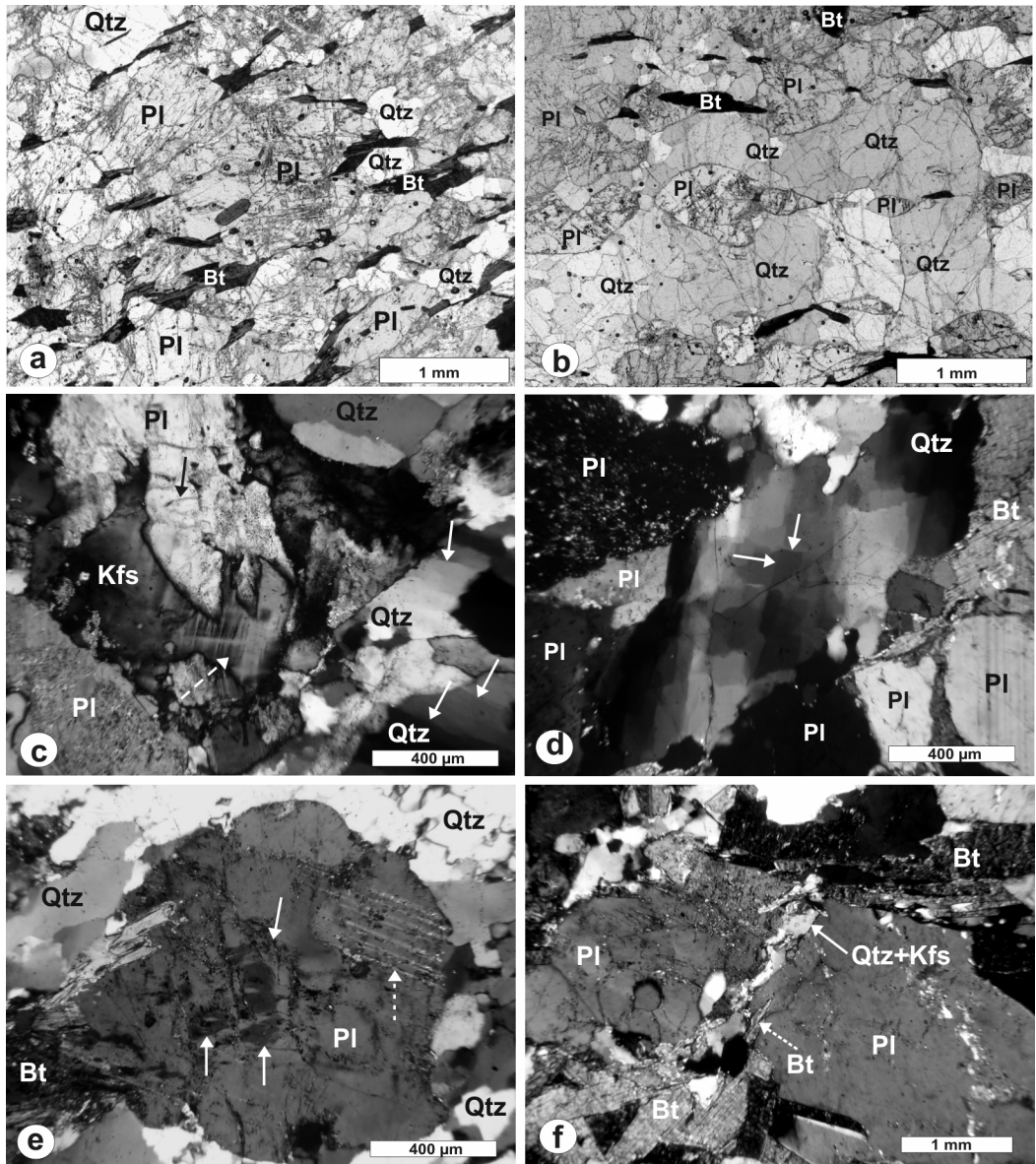


Fig. 3. Microstructural relations of rock-forming minerals in orthogneiss samples E216A, E205A, E196, E166, E202: a) curved and thinner biotite flakes, PPL; b) lens-shaped plagioclase grains surrounded by re-crystallized quartz, PPL; c) prismatic extinction in quartz (white arrows), myrmekitic plagioclase (black arrow) and cross-hatched microcline twinning in anherd K-feldspar (dashed arrow), CPL; d) 'chessboard' pattern in quartz (arrows), CPL; e) rounded plagioclase grain with wedge-shaped plagioclase twinning (dashed arrow) and irregular-shaped antiperthites (white arrows), CPL; f) plagioclase cracks filled with quartz, K-feldspar (arrow) and biotite (dashed arrow), CPL

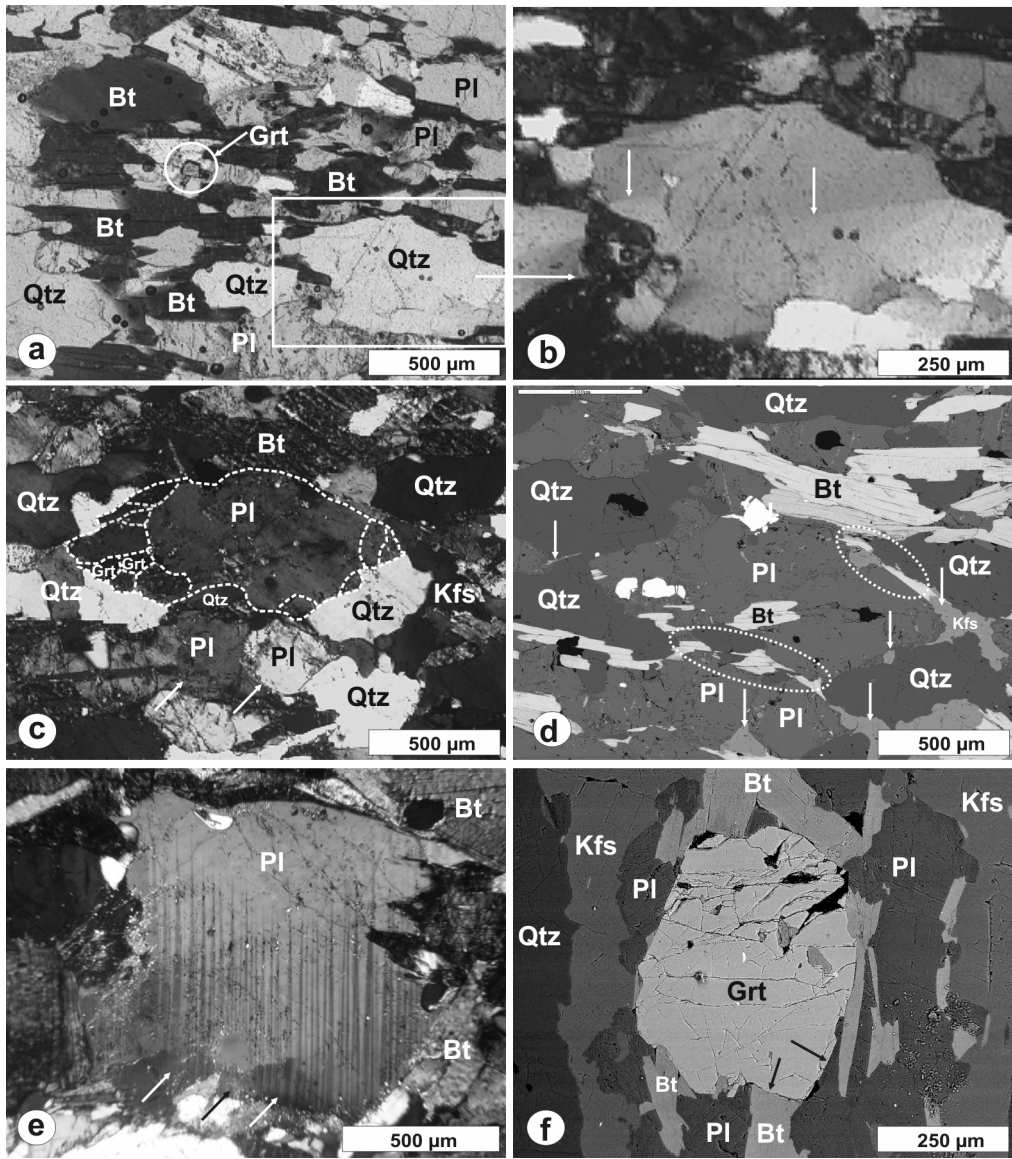


Fig. 4. Microstructural relations of rock-forming minerals in paragneiss sample E168A: a) elongated and extended biotite flakes forming continuous foliation, PPL; b) prismatic extinction in quartz, CPL; c) ‘core-mantle’ structure in plagioclase (dashed lines) and small rounded plagioclase grains (arrows), CPL; d) interstitial and in pressure shadows K-feldspar (white arrows); dynamic recrystallized fine-grained quartz, biotite and K-feldspar round large plagioclase grains (dashed ellipses), BSE; e) wedge-shaped plagioclase twinning and subgrains (arrows), CPL; f) euhedral garnet grain and sharp and clean boundaries with plagioclase and biotite (arrows), BSE

(~0.5 mm) are elongated, parallel to the general foliation (Fig. 4f) and display undulose extinction. Some of them partially or completely include small plagioclase grains full of myrmekites.

Garnet grains are small (up to 1 mm), euhedral to subhedral, slightly rounded (Fig. 4f). They occur predominantly near biotite flakes which in some cases penetrate into garnet cracks.

Microstructures reflect deformation at high-grade amphibolite facies metamorphism ca. 600°C: undulose to prismatic extinction in quartz (Fig. 4b); ‘core-mantle’ textures in plagioclase (Fig. 4c); wedge-shaped plagioclase twinning (Fig. 4e) (Passchier & Trouw 1996; Kruhl 1996). Dynamically re-crystallized fine-grained quartz and/or K-feldspar and plagioclase occur along plagioclase grain boundaries (Fig. 4d) and support an interpretation of partial melting processes influence (Mehnert et al. 1973; Jurewicz & Watson 1984; Sawyer 1999). These features coincide with field observation of initial stage of migmatization in paragneisses.

Garnet, plagioclase and biotite grain contacts testify for equilibrium relations with each other. The contact lines are sharp and smooth and show no evidence of replacement of one mineral by another or new phase crystallization (Fig. 4f). The mentioned microstructure criteria imply for a simultaneous coexistence of chemically compatible minerals (Vernon 1977).

Amphibolites

The major mineral assemblage consists of amphibole and plagioclase. There is also minor quartz and secondary biotite. The accessory minerals are titanite, magnetite, apatite and zircon. The term “amphibolite” is used in accordance with the mineral composition and macroscopic characteristics, without, as far as possible, any genetic connotation as recommended by Coutinho et al. (2007).

Amphibole (<1.5–2 mm) is subhedral to anhedral, exhibiting dark green to light green

pleochroism. Larger plagioclase grains (1–1.5 mm) are subhedral with undulose extinction, while smaller grains (~0.5–1 mm) are anhedral, rounded to lens-shaped. Some large amphibole and plagioclase grains contain inclusions of euhedral plagioclase and amphibole respectively (Fig. 5).

Elongated quartz aggregates occur parallel to the foliation. Rare anhedral interstitial quartz grains display weak undulose extinction.

Biotite (<1 mm) with dark brown to light yellow pleochroism is rare. The biotite contacts with amphibole grains are sharp and smooth,

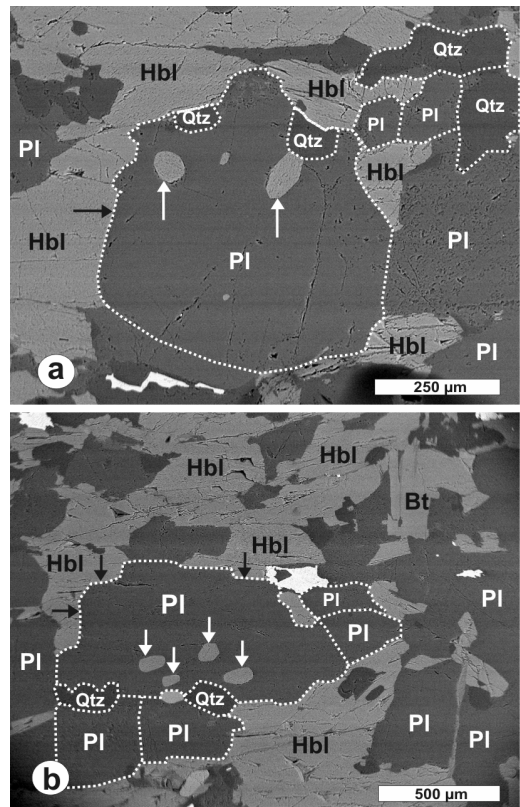


Fig. 5. Microstructural relations between rock-forming minerals in metabasite sample E209: a) and b) subhedral plagioclase with small euhedral amphibole inclusions (white arrow); sharp and new-phase-free boundaries between Pl and Hbl (black arrow), BSE

but near plagioclase and quartz biotite flakes are irregular and ragged in shape.

The microstructural relations refer to deformation at amphibolite facies conditions (Vernon 1975; Voll 1976; Tullis 1983), namely: plagioclase undulose extinction due to microcracks and subgrain formation; and wedge-shaped plagioclase twinning. Triple junctions of polygonal plagioclase crystals reflect plagioclase re-crystallization by means of complete consumption of parental larger crystals at static conditions (Srivastava & Mitra 1996).

Plagioclase-amphibole boundaries are usually sharp and smooth showing no evidence of mutual replacement or new phase crystallization (Fig. 5). These microstructural features suggest simultaneous coexistence of compatible plagioclase and amphibole (Vernon 1977).

Mineral chemistry

The orthogneisses have homogeneous plagioclases of oligoclase-andesine composition (An_{28-33} ; Appendix: Table 1). K-feldspar grains show normal compositional zoning from Or_{86} in the core to Or_{91} in the rim and Or_{89-92} in smaller grains (Appendix: Table 2).

Biotite is Fe-rich with high $Fe/(Fe+Mg)$ ratio value (0.53-0.60) and low Al^{IV} contents (2.36-2.52 *apfu*) corresponding to annite component enrichment (Appendix: Table 3). The content of TiO_2 in biotite varies from 2.9 to 4.5% and correlates positively with $Fe/(Fe+Mg)$ ratio values. The biotites studied have similar compositions with those from biotite gneisses of the Startsevo unit (Egri dere) and Madan unit along the Vacha river valley (Cherneva et al. 1997).

The paragneisses contain homogeneous plagioclase grains of oligoclase-andesine composition (An_{27-32}), which Ca contents increase (An_{35-39}) close to adjacent garnet grains (sample E168A, from points 5'l-g to 14l-g; Appendix: Table 1), due to Ca diffusion re-equilibration between garnet and plagioclase. Minor amount of interstitial and pressure shadowed K-feldspars as well as larger K-feldspar grains have high Or_{-

component (Or_{86-90}) and low Ab-component (Ab_{13-09} ; Appendix Table 2).

Biotite compositions have $Fe/(Fe+Mg)$ ratio values (0.51-0.60) similar to biotite in orthogneisses, and larger Al^{IV} variation (2.36-2.62 *apfu*, Appendix: Table 3). There is not systematic compositional distinction between large and small (recrystallized) biotite grains. The content of TiO_2 (1.7-3.3 %) is lower than TiO_2 in orthogneiss biotite. The paragneiss biotite resembles biotite composition of Kanarata shear zone metapelites (Georgieva et al. 2002) situated between Arda and Startsevo units.

Garnet composition is almandine dominated with relatively high and constant spessartine component (XSp 0.13-0.18) (Appendix: Table 4). The grossular component increases from core to rim (XGr from 0.09 to 0.25) while the almandine and pyrope components decrease ($XAld$ from 0.63 to 0.53 and $XPyr$ from 0.12 to 0.06). The $Fe/(Fe+Mg)$ ratio values increase in the same direction (from 0.84 to 0.90) or keep constant values (Appendix: Table 4). The garnet rim next to biotite is poorer in Fe and Mg- and richer in Ca when compared with garnet rims close to plagioclase grains. The explanation refers to experimental results of slower Ca diffusion during retrograde re-equilibration (Vielzeuf et al. 2007).

The amphibolites comprise homogeneous plagioclase grains of andesine composition (An_{34-37} ; Appendix: Table 1). Plagioclase rims near rare biotite flakes show decrease of An-component (to An_{01}). Very small, anhedral K-feldspar grains (Or_{96} , Ab_{04}) occur between acid plagioclase and biotite suggesting local re-equilibration related to biotite formation.

Biotites from amphibolites differ with lower $Fe/(Fe+Mg)$ ratio values (from 0.40 to 0.43) and higher Al^{IV} contents (2.66-2.67 *apfu*; Appendix: Table 3) when compared with biotites from ortho- and paragneisses.

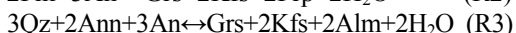
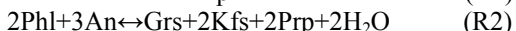
Amphibole has tschermakite composition according to the nomenclature of Leake et al. (1997, 2003). The large crystals display core to rim decrease of Ti (0.13 to 0.08 *apfu*) and small increase of Na (0.36 to 0.44 *apfu*), K (0.09 to 0.14 *apfu*), and Al (2.10 to 2.22 *apfu*)

(Appendix: Table 5). Amphibole inclusions in plagioclase have similar contents of Si, Al, Ti, Mn, Ca and Fe²⁺ like large amphibole cores. The enrichment of Na and K in amphibole rims is due to faster diffusion of alkali elements through crystal lattice during diffusion re-equilibration.

Thermobarometry of paragneisses

The paragneiss mineral assemblage is appropriate to determine the *P-T* metamorphic conditions using garnet-plagioclase and garnet-biotite equilibrium pairs whose relations suit the requirements of equilibrium mineral assemblage according to metamorphic petrology microstructural criteria (Vernon 1977; Bucher & Frey 2002; Vernon & Clarke 2008). Selected biotite flakes have ‘clean’ peripheries and cleavage system. The garnet, plagioclase and biotite contacts are smooth and ‘clean’, with no evidence of minerals interaction and replacement or new phase formation showing metamorphic conditions in equilibrium (Fig. 4f).

The TWQ software calculations of Mg, Fe and Ca equilibrium distribution between garnet, biotite and plagioclase offer the following reactions:



The intersection points of R1, R2 and R3 reaction curves correspond to *P-T* values in the temperature interval 630–655°C at pressures from 0.88 to 0.96 GPa for equilibrium assemblage composed of garnet rims, and adjacent large biotite and plagioclase grains (Fig. 6). The participation of smaller biotite and plagioclase grains in association with garnet rims yield higher *P-T* values above 720–740°C at ~1 GPa.

The above reactions allow an application of conventional thermobarometry based on Mg-Fe exchange between garnet and biotite and Ca-exchange between garnet and plagioclase. The popular Fe-Mg exchange garnet-biotite thermometers put some limits regarding mineral chemistry of the pairs,

namely: (Ca+Mn)/(Ca+Mn+Fe+Mg) ratio values up to ~0.2 in garnet and (Al^{VI}+Ti)/(Al^{VI}+Ti+Fe+Mg) up to ~0.15 in biotite (Ferry & Spear 1978); (XGrs)³ > 0.03 in garnet and Al^{VI}/(Al^{VI}+Ti+Fe+Mg) > 0.03 in biotite (Wu et al. 2004). Our data meet the requirements of several thermometers (Hodges & Spear 1982; Dasgupta et al. 1991; Thompson 1976; Perchuk & Lavrent'eva 1983; Holdaway & Lee 1977). We have used also the geothermobarometer of Caddick & Thompson (2008) for pressure estimates.

The garnet-biotite-plagioclase thermobarometer of Caddick & Thompson (2008) defines a temperature range of 630–670°C at pressures from 0.99 to 1.23 GPa (Table 6; Fig. 9). Similar temperature values in the range of 600–660°C yield the garnet-biotite thermometers of Hodges & Spear (1982) and Dasgupta et al. (1991) at given pressures from 0.99 to 1.23 GPa (Table 6; Fig. 9). The temperature estimates obtained from the other garnet-biotite thermometers are close to or below 600°C (Table 6; Thompson 1976; Perchuk & Lavrent'eva 1983; Holdaway & Lee 1977).

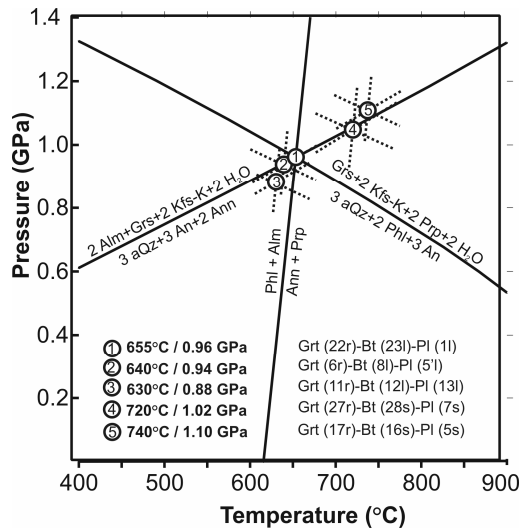


Fig. 6. Thermobarometric estimates using TWQ software (Berman 1991) and thermodynamic database of Berman (1992) with equilibrium reactions

Table 6. Thermobarometric estimates of selected garnet-plagioclase and garnet-biotite pairs

Pairs	Garnet	22 r	17 r	27 r	6 r	11 r
	Plagioclase	11	5 s	7 s	‘51	131
	Biotite	231	16 s	28 s	81	121
P (GPa) after Caddick & Thompson (2008)	600°C	1.03	1.02	0.96	1.04	0.91
	650°C	1.16	1.15	1.08	1.17	1.04
	700°C	1.29	1.28	1.21	1.30	1.17
T (°C) after Caddick & Thompson (2008)	0.9 GPa	649	763	755	633	623
	1.1 GPa	661	775	767	645	635
	1.3 GPa	673	787	779	657	647
T (°C) after Hodges & Spear (1982)	0.9 GPa	643	763	755	633	620
	1.1 GPa	650	771	763	640	627
	1.3 GPa	657	779	771	646	633
T (°C) after Dasgupta et al. (1991)	0.9 GPa	643	770	731	609	598
	1.1 GPa	652	780	742	618	607
	1.3 GPa	661	790	752	627	616
T (°C) after Thompson (1976)	0.9 GPa	613	689	696	585	587
	1.1 GPa	627	704	711	599	601
	1.3 GPa	641	720	726	613	614
T (°C) after Perchuk & Lavrent'eva (1983)	0.9 GPa	586	638	642	567	568
	1.1 GPa	591	643	648	572	573
	1.3 GPa	596	649	654	577	578
T (°C) after Holdaway & Lee (1977)	0.9 GPa	582	647	653	559	560
	1.1 GPa	589	654	660	565	567
	1.3 GPa	595	661	667	572	573

Thermobarometry of amphibolites

The *amphibolite* mineral assemblage offer a possibility to define *P-T* conditions based on Ca-Al-Si exchange between amphibole and plagioclase. Selected pairs represent three types of relations: 1) between subhedral amphibole and plagioclase rims, 2) between subhedral amphibole and plagioclase cores and 3) small euhedral amphibole inclusions and host subhedral plagioclase. The grain contacts are smooth and ‘clean’ in the three cases (Fig. 5).

The Al/Si ratio values in amphibole-plagioclase pairs are pressure dependent (Fershtater 1990). The Al/Si ratio values in large subhedral amphibole grains as well as in small euhedral amphibole inclusions vary from 0.327 to 0.344 (Appendix: Table 5). The Al/Si ratio values in plagioclase vary from 0.511 to 0.526 (Appendix: Table 1). The Al/Si distribution between amphibole and plagioclase corresponds to

equilibrium at about 0.6 GPa (Fig. 7).

According to Al-in-amphibole geobarometers of Hammarstrom & Zen (1986), Hollister et al. (1987) and Schmidt (1992)

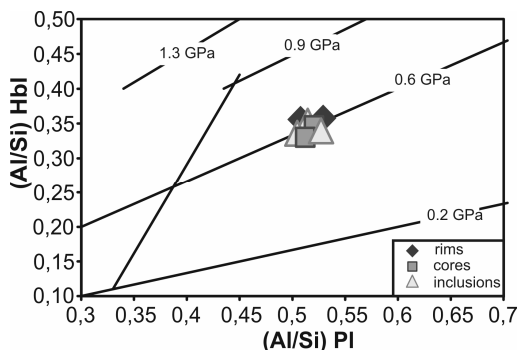


Fig. 7. Al/Si distribution between equilibrium coexisting amphibole and plagioclase from the amphi-bolite sample E209 after Fershtater (1990)

Table 7. Thermobarometric estimates of selected amphibole-plagioclase pairs

Pairs	Amphibole Plagioclase	No No	3 r 2 r	7 r 8 r	4 c 1 c	6 c 9 c	5 i 1 c	11 i 10 ni	12 i 13 ni
P (GPa)	Schmidt (1992)		0.75	0.75	0.70	0.74	0.73	0.71	0.72
	Hammarstrom & Zen (1986)		0.71	0.72	0.67	0.71	0.70	0.68	0.65
	Hollister et al. (1987)		0.79	0.80	0.74	0.78	0.78	0.75	0.76
P (GPa)	Bhadra & Bhattacharya (2007) at 640°C		0.78 0.81	0.57 0.62	0.69 0.74	0.72 0.77	0.69 0.72	0.43 0.48	0.32 0.38
	Bhadra & Bhattacharya (2007) at 720°C		0.99 0.98	0.81 0.83	0.88 0.89	0.93 0.94	0.90 0.90	0.66 0.69	0.59 0.61
T°C	Holland & Blundy (1994) at P min		683 692	637 674	682 710	659 687	676 698	658 692	630 718
	Holland & Blundy (1994) at P max		709 700	661 684	699 711	681 695	695 703	686 697	663 721
	Holland & Blundy (1994) at P after Fershtater (1990)		673 689	640 675	676 710	649 683	669 696	673 695	651 720

calculated pressures range from 0.65 to 0.80 GPa (Table 7). The Al-in-amphibole geobarometers although for magmatic rocks, are used here because the studied amphibolites are supposed to have magmatic protolith origin (Raeva 2009).

The garnet-free amphibolite mineral assemblage is appropriate for hornblende-plagioclase geobarometer of Bharda & Bhattacharya (2007) formulated for metamorphic pressure estimating of medium to high-grade metabasic rocks. The results expand the pressure range from 0.57 to 0.99 GPa (Table 7; Fig. 9). The pressures calculated below 0.5 GPa suppose disequilibrium amphibole-plagioclase pairs.

The temperature estimates of the amphibolites are calculated according to the amphibole-plagioclase geothermometer of Holland & Blundy (1994) with additional corrections recommended by Dale et al. (2000) at pressure values according to Fershtater (1990), Hammarstrom & Zen (1986), Hollister et al. (1987), Schmidt (1992) and Bharda & Bhattacharya (2007) (Table 7). The thermometric results range from 640 to 720°C at pressures from 0.57 to 0.99 GPa for all types of amphibole-plagioclase pairs (Fig. 9).

Two-feldspar thermometry

The orthogneiss mineral assemblage allows application of two-feldspar geothermometer. We have used the method of Fuhrman & Lindsley (1988) through SOLVCALC program package (Wen & Nekvasil 1994). The microstructural relations suggest several types of equilibrium pairs of plagioclase and K-feldspar: cores of large subhedral grains; rims of adjacent large subhedral grains; small anhedral adjacent grains; and large grain rims with adjacent small grains. The thermometric calculations at 0.3, 0.5 and 0.7 GPa yield equilibrium temperatures in the range of 524 to 592°C for large grains core-core pairs and 528–552°C for small anhedral grain pairs. The similarity of these results suggests common feldspar re-equilibration during post-migmatitic ductile deformation. The temperatures obtained from the other pair types are even lower (445–510°C; Table 8).

Calculated compositions of equilibrium feldspar pairs differ from the real ones with higher Ab- and lower Or-component (both by 1 to 3.5%) in K-feldspar, and slightly higher (by 0.1 to 0.3%) Or-component in the plagioclase. The Ab-exsolution observed in K-feldspar

Table 8. Temperature estimates of selected plagioclase-K-feldspar pairs from orthogneisses

Sample	Pairs (Pl-Kfs)	3 GPa	5 GPa	7 GPa
E159A	9 c - 12 c	571	573	592
E171	4 c - 1 c	484	524	529
E171	14 s - 15 s	522	528	529
E171	21 s - 9 s	544	551	552
E171	3 r - 2 r	492	510	525
E173	9 r - 8 s	469	478	481
E166	2 r - 21 s	470	477	495
E166	2 r - 22 s	445	510	523

support an interpretation of deformational induced microperthite formation and retrogressive re-equilibration of feldspar compositions.

Structural state of K-feldspars

The results of X-ray diffraction analysis of K-feldspar mineral fractions from ortho- and paragneisses are shown in Table 9. The amount of Al in 2T1 sites in K-feldspar structure vary in the range from 0.78 to 0.81. Al proportions between T1 (o) and T1 (m) positions are equal with calculated triclinicity (Δp) of 0. There is slight increase of Al in T1 (o) position in limited number of samples, the triclinicity of which reaches up to 0.1 (Table 9, Fig. 8). The triclinicity values from 0 to 0.1 and the coefficient of order ((T1(o)-0.25)/0.75) from 0.19 to 0.27 correspond to orthoclase structure of K-feldspars (Wright 1968).

The orthoclase structural state of K-feldspars is characteristics for migmatitic units in the Central Rhodopes (the Arda and the Madan unit along the Vacha river valley) whereas K-feldspars from the lower-grade nonmigmatitic ones (Asenitsa unit) have dominantly microcline structures (Arnaudova et al. 1990). According to cited authors the orthoclase-microcline structural transition spans the temperature range 500-550°C in the Asenitsa unit metamorphic rocks. Irregular appearance of cross-hatched microcline twinning in K-feldspar from orthogenisses in the

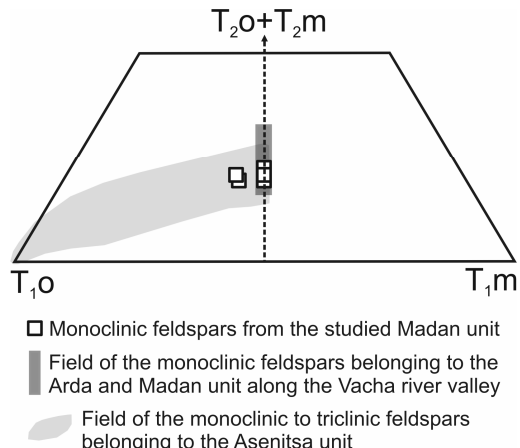


Fig. 8. Al occupancy of tetrahedral sites in alkali feldspars after Stewart & Wright (1974); data for K-feldspars from the Asenitsa, Arda and Madan unit along the Vacha river valley after Arnaudova et al. (1990)

region of the Smilyan shear zone refers to the influence of synmetamorphic subsolidus deformation processes at decreasing temperature. X-ray diffraction study of K-feldspars from the Smilyan pluton indicates orthoclase structural state of K-feldspars everywhere in the granite body with triclinicity values (Δp) equal to zero (Belmustakova 1995).

Table 9. Al occupancy of tetrahedral sites in K-feldspars from the Madan unit orthogneisses and paragneiss E163 according to Wright (1968)

Sample	Δp	T1(o)	T1(m)	T1(o)+ T1(m)	T2(o)= T2(m)
E163	0.00	0.40	0.40	0.79	0.10
E149	0.00	0.41	0.41	0.81	0.10
E165	0.00	0.41	0.41	0.81	0.10
E166	0.10	0.45	0.35	0.79	0.10
E171	0.10	0.46	0.36	0.81	0.10
E159A	0.00	0.39	0.39	0.78	0.11
E174	0.00	0.40	0.40	0.80	0.10
E175	0.00	0.40	0.40	0.81	0.10
E196	0.00	0.40	0.40	0.79	0.10
E216A	0.11	0.45	0.34	0.79	0.10

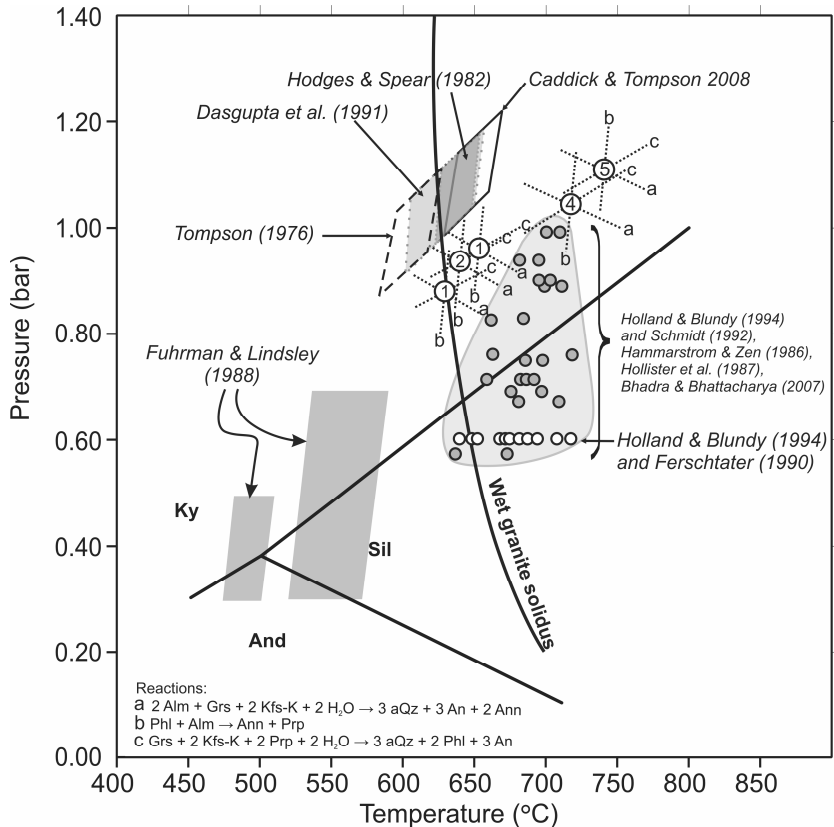


Fig. 9. Thermobarometric results for paragneisses and amphibolites; Ky-Sil-And stability fields after Holdway (1971); wet granite solidus after Johannes (1984); equilibrium triple points between Grt-Bt-Pl after TWQ software (Berman 1991)

Discussion

The thermobarometric results characterize the stage of mineral re-equilibration in orthogneisses, paragneisses and amphibolites during retrograde metamorphic path in the Madan unit along the Arda river valley.

Most of the temperature values for paragneisses cluster together around the water-saturated granite solidus (Fig 9) in conformity with field features of an initial stage of migmatization (metatexis) in the Madan unit gneisses. The temperature range of 600 to 670°C obtained from the geothermometers of Caddick & Thompson (2008), Hodges & Spear (1982), Dasgupta et al. (1991) and TWQ

software, characterize the most probable thermal equilibrium in the metamorphic rocks that crop out to the West of the Smilyan granite (Fig. 2). Higher temperature estimates above 700°C are calculated for pairs of garnet rim and small biotite grains (Figs. 6, 9).

Temperatures far above the wet granite solidus are not consistent with field and microstructural observations of metatexite type of migmatization due to initial stage of low-temperature melting. Some local compositional deviations in garnet (higher Mg and lower Mn) close to adjacent small biotite (Fe^{2+} lower than in large biotites) suggest incomplete equilibration in spite of microstructural evidence of compatible mineral coexistence.

The calculated temperature range of 640-720°C for the amphibolites is higher than that for the paragneisses. A thermal influence of syn- to postmetamorphic granite magma emplacement could be supposed for the eastern part of the Madan unit. The abundant small granite bodies and observed local transitional eastern contacts of the Smilian granite with the host metamorphic rocks support this interpretation.

The obtained metamorphic temperature conditions of the Madan unit along the Arda river valley are similar with these of the Startsevo and Madan unit along the Vacha river valley (Ovcharova 2004; Cherneva et al. 1995).

Microstructural features of the rocks reflect the thermal conditions of synmetamorphic deformation and corresponding mineral recrystallization. Sarov et al. (2005) consider subgrain formation in large K-feldspars, undulose extinction in plagioclase and thin quartz ribbons in orthogneisses of the same area as results of ductile deformation processes. The cited authors observe in local shear zones or in interstices fine-grained, thin aggregates of plagioclase, quartz and biotite controlled by orientated tension and suppose that its formation is due to a ductile deformation in a great depth and fluid presence.

Our observations of undulose to prismatic extinction and ‘chessboard’ pattern in quartz, ‘core-mantle’ structures in plagioclases and K-feldspars as well as undulose extinction in K-feldspars from ortho- and paragneisses suggest metamorphic conditions ca. 600-650°C close to the wet granite solidus in accordance with the indicators defined by Kruhl (1996), Passchier & Trouw (1996), Albertz (2006). The mentioned microstructures are typical for deformed and re-equilibrated rocks during retrograde cooling and correspond to the temperature estimate obtained from conventional thermometry.

The orthoclase structure of K-feldspars in ortho- and paragneisses correspond to the temperature range around the wet granite solidus. The local appearance of cross-hatched microcline twinning in K-feldspars from the orthogneisses in the Smilyan shear zone area

has microstructural evidence of deformation origin. The temperature range of 520-590°C and lower (450-510°C) for the orthogneisses obtained from the two-feldspar thermometer of Fuhrman & Lindsley (1988) overlap the orthoclase-microcline structural transition (Stewart & Wright 1974). The temperature results refer to thermal re-equilibration after orthoclase crystallization without destroying the mineral structure.

The pressure results for the paragneisses vary in the extended range from 0.88 to 1.23 GPa and differ from the pressure estimate in the range of 0.57-0.99 GPa for the amphibolites. The pressure variation could be an effect of different erosion levels, namely: lower level for paragneisses that crop out to the North-West of the Smilyan pluton; and higher level for amphibolites situated to the South-East of the pluton. The hypsometric difference between the two levels according to the calculated pressure estimates amounts to 7-11 km. The calculated pressure difference is acceptable having in mind the horizontal distance of about 20 km between paragneiss and amphibolite outcrops and the gneiss foliation dip of 25-30° (Fig. 2). Furthermore, the different types of rocks used for thermobarometry belong to different geochemical systems: K-Na-Ca-Al-Si for paragneisses and Fe-Mg-Ca-Al-Si for amphibolites. Good concomitant verification of the above hypothesis would be additional studies of metabasic rocks from the western part of the Madan unit.

Conclusions

The field relationships and the mineral assemblages of the Madan unit metamorphic rocks reveal a retrogressive regional metamorphic evolution during and after syn- to postkinematic granite magma emplacement. Conventional thermobarometry shows upper amphibolite facies P - T metamorphic conditions of 600-670°C/ 0.9-1.2 GPa for the paragneisses and 640-720°C/0.6-1.0 GPa for the amphibolites. The temperatures are in accordance with field observations of initial stage of

migmatization (metatexis), microstructural features and orthoclase structure of K-feldspars. Lower $P-T$ conditions towards 520–590°C/0.3–0.7 GPa favoured subsolidus and solidus re-equilibration during synmetamorphic ductile deformation. The obtained thermobarometric results are similar with these for the Startsevo and Madan unit along the Vacha river valley.

Acknowledgements: The National Science Fund of the Ministry of Education and Science in Bulgaria has supported this work financially by project № BY-H3-05/05. The authors thank Tsveta Stanimirova for the structural analyses of the K-feldspars and Tzvetoslav Iliev for his help with microprobe analyses.

References

- Arkadaskiy S, Böhm C, Heaman L, Cherneva Z, Stancheva E (2000) New U-Pb age results from the Central Rhodope Mts., Bulgaria: ABCD – GEODE Workshop, Borovets, Bulgaria, p.5
- Arkadaskiy S, Böhm C, Heaman L, Ovtcharova M, Cherneva Z, Stancheva E (2003) Remnants of Neoproterozoic oceanic crust in the Central Rhodope metamorphic complex, Bulgaria. *The Geological Society of America Vancouver Annual Meeting*, GS3-62
- Albertz M (2006) Relationships between melt-induced rheological transitions and finite strain: observations from host rock pendants of the Tuolumne Intrusive Suite, Sierra Nevada, California. *Journal of Structural Geology*, **28**, 1422–1444
- Arnaudov V, Amov B, Baldjieva T, Pavlova M (1990a) Tertiary magmatic pegmatites in the Rhodope crystalline complex. Uranium-lead zircon dating. *Geologica Balcanica*, **20.6**, 25–32
- Arnaudov V, Amov B, Cherneva Z, Arnaudova R, Pavlova M, Bartnitsky E (1990b) Petrological-geochemical and lead-isotope evidence of Alpine metamorphism in the Rhodope crystalline complex. *Geologica Balcanica*, **20**, 5, 29–44
- Arnaudova R, Cherneva Z, Stancheva E (1990) Structural state and geochemical characteristics of potassic feldspars from the Central Rhodope metamorphic complex. *Geologica Balcanica*, **20**, 1, 67–84
- Belmustakova H (1995) Petrology of the Smilyan pluton (Central Rhodopes) and its metamorphic frame. *Review of the Bulgarian Geological Society*, **56**, 1, 75–91 (in Bulgarian)
- Berman RG (1991) Thermobarometry using multi-equilibrium calculations: A new technique with petrological applications. *Canadian Mineralogist*, **29**, 833–855
- Berman RG (1992) Thermobarometry with estimation of equilibrium state (TWEEQU): an IBM-compatible software package. *Geological survey of Canada open file* 2534
- Blumenfeld P, Bouchez JL (1988) Shear criteria in granite and migmatite deformed in the magmatic and solid states. *Journal of Structural Geology*, **10**, 361–372
- Bouchez JL, Delas C, Gleizes G, Nedelev A, Cuney M (1992) Submagmatic microfracture in granites. *Geology*, **20**, 35–38
- Bucher K, Frey M (2002) Petrogenesis of metamorphic rocks. 7th ed, New York, Springer-Verlag, 341 p.
- Caddick MJ, Thompson AB (2008) Quantifying the tectono-metamorphic evolution of politic rocks from wide range of tectonic settings: mineral compositions in equilibrium. *Contributions to Mineralogy and Petrology*, **156**, 177–195
- Carrigan CW, Mukasa SB, Essene EJ, Haydutov I, Kolcheva K (2006) Multiple P-T path for eclogites from the Bulgarian Rhodope Massif. In: *GSA Philadelphia Annual Meeting*, October 22–25, 2006
- Cherneva Z, Arnaudova R, Iliev Tz, Rekalov K (1997) Feldspar thermometry of migmatic formations from the Central Rhodopes, *Review of the Bulgarian Geological Society*, **58**, 3, 139–156 (in Bulgarian)
- Cherneva Z, Dimov D, Stancheva E, Daieva L (1995) Sobsolidus and anatetic vains in migmatic gneisses from the Vacha-river valley, Central Rhodopes, *Review of the Bulgarian Geological Society*, **56**, 3, 91–109 (in Bulgarian)
- Cherneva Z, Georgieva M (2007) Amphibole-bearing leucosome from the Chepelare area, Central Rhodopes: P-T conditions of melting and crystallization. *Geochemistry, Mineralogy and Petrology*, **45**, 79–95.
- Cherneva Z, Georgieva M, Stancheva E, Gerdjikov I (2008) High pressure garnet-bearing migmatite from the Chepelare area, Central Rhodopes. *Geologica Balcanica*, **37**, 1–2, 47–52
- Coutinho JMV, Kräutner HG, Sassi FP, Schmid R, Sen S (2007) A systematic nomenclature for metamorphic rocks: 8. Amphibolite and granulite. Recommendations by the IUGS

- Subcommission on the Systematics of Metamorphic Rocks. Recommendations, web version of 01.02.2007.
www.bgs.ac.uk/scmr/home.html, 12 p
- Dale J, Holland T, Powell R (2000) Hornblende-garnet-plagioclase thermobarometry: a natural assemblage calibration of the thermodynamics of hornblende. *Contributions to Mineralogy and Petrology*, **140**, 353-362
- Dasgupta S, Sengupta P, Guha D, Fukuoka M (1991) A refined garnet-biotite Fe-Mg exchange geothermometer, and its application in amphibolites, and granulites. *Contributions to Mineralogy and Petrology*, **109**, 130-137
- Dimitrov Str (1955) State and subsequent problems and study of magmatic and metamorphic complexes in Bulgaria. *Proceedings of Academy of Sciences of URSS, Geology series*, **1**, 5, 5-15 (in Russian)
- Fershtater GB (1990) An empirical plagioclase-hornblende barometer. *Geochemistry*, **3**, 328-335
- Ferry JM, Spear FS (1978) Experimental calibration of the partitioning of Fe and Mg between biotite and garnet. *Contributions to Mineralogy and Petrology*, **66**, 113-117
- Fitz Gerald JD, Stunitz H (1993) Deformation of granitoids at low metamorphic grade. I: Reactions and grain size reduction. *Tectonophysics*, **221**, 269-297
- Fuhrman ML, Lindsley DH (1988) Tertiary-feldspar modeling and thermometry. *American Mineralogist*, **73**, 201-215
- Georgieva M, Cherneva Z, Kolcheva K, Sarov S, Gerdjikov I, Voinova E (2002) P-T metamorphic path of sillimanite-bearing schists in an extensional shear zone, Central Rhodopes, Bulgaria. *Geochemistry, Mineralogy and Petrology*, **39**, 95-106
- Georgieva M, Cherneva Z, Mogessie A, Stancheva E (2007) Garnet-kyanite schists from the Chepelare area, Central Rhodope Mts., Bulgaria: mineral chemistry, thermobarometry and indications for high-pressure melting. *Annual Scientific Conference of BGS "Geosciences 2007"*, 97-98
- Guiraud M, Ivanov Z, Burg JP (1992) Discovery of high pressure schists in the region of Byala Tcherkva (Central Rhodopes, Bulgaria). *Reports of Academy of Sciences, Paris*, **315**, series II, 1695-1702 (in French)
- Hammarstrom JM, Zen E (1986) Aluminium in hornblende: an empirical igneous geobarometer. *American Mineralogist*, **71**, 1297-1313
- Hodges KV, Spear FS (1982) Geothermometry, barometry and the Al₂SiO₅ triple point at Mt. Moosilauke, New Hampshire. *American Mineralogist*, **67**, 1118-1134
- Holdaway MJ (1971) Stability of andalusite and the aluminum silicate phase diagram. *American Journal of Science*, **271**, 97-131.
- Holdaway MJ, Lee SM (1977) Fe-Mg cordierite stability in high grade pelitic rocks based on experimental, theoretical and natural observations. *Contributions to Mineralogy and Petrology*, **63**, 175-198
- Holland T, Blundy J (1994) Non-ideal interactions in calcic amphiboles and their bearing on amphibole-plagioclase thermometry. *Contributions to Mineralogy and Petrology*, **116**, 433-447
- Hollister LS, Grissom GC, Peters EK, Stowell HH, Sisson VB (1987) Confirmation of the empirical correlation of Al in hornblende with pressure of solidification of calc-alkaline plutons. *American Mineralogist*, **72**, 231-239
- Ichev M (1994) Eclogites amphibolitises dans la composition de la Formation de Lukovitsa de la partie septentrionale des Rhodopes Centrales. *Comptes Rendus de l'Academie Bulgare des Sciences*, **47**, 5, 49-52
- Ivanov Z (1998) Tectonics of Bulgaria. *Academic work at Sofia University "St. Kliment Ohridski"*, 675 p. (in Bulgarian)
- Ivanov Z, Moskovski S, Kolcheva K (1979) Fundamental characteristics of the structure in the central parts of the Rhodope massif. *Geologica Balcanica*, **9**, 1, 3-50 (in Russian)
- Ivanov Z, Moskovski S, Dimov D, Kolcheva K (1980) Litostratigraphic subdivision of metamorphic rocks in the autochthonous complex in the Central Rhodopes between Chepelare river upper valley and Vacha river valley. *Geologica Balcanica*, **10**, 3, 3-29 (in Russian)
- Ivanov Z, Moskovski S, Kolcheva K, Dimov D, Klain L (1984) Geological structure of the Central Rhodopes. I. Lithostratigraphic subdivision and features of the section of metamorphic rocks in the northern parts of Central Rhodopes. *Geologica Balcanica*, **14**, 1, 3-42 (in Russian)
- Ivanov Z, Dimov D, Dobrev S, Kolkovski B, Sarov S (2000) Structure, Alpine evolution and mineralizations of the Central Rhodopes area (South Bulgaria). *Guide to Excursion (B)*,

- ABCD-GEODE 2000 Workshop, Borovets, Bulgaria.* 50p.
- Johannes W (1984) Beginning of melting in the granite system Qz–Or–Ab–An–H₂O. *Contributions to Mineralogy and Petrology*, **86**, 264–273
- Jurewicz SR, Watson EB (1984) Melt coalescence in a felsic system: The importance of surface energy. *Contributions to Mineralogy and Petrology*, **85**, 25–29
- Kaiser-Rohrmeier M (2005) Age and geodynamic evolution of hydrothermal vein deposits in the Madan extensional complex (Bulgaria), *Unpublished PhD Thesis, Diss ETHNr. 15878, ETH Zurich*, 141 pp
- Katskov N (1962) Report for geological mapping and ore deposit prospecting in the middle parts of the Central Rhodopes and in the Arda river spring parts in 1:25 000 scale during 1961, **I, V–8** (in Bulgarian)
- Kolcheva K, Zeljazkova-Panajotova M, Dobrev N, Stojanova V (1986) Eclogites in Central Rhodope metamorphic group. *Geochemistry, Mineralogy and Petrology*, **20–21**, 130–144
- Kostov I, Grozdanov L, Petrusenko S, Krasteva M, Rashkova D (1986) Sin- and post-metamorphic mineralizations in the Central Rhodopes. *Geochemistry, Mineralogy and Petrology*, **20–21**, 25–48 (in Bulgarian)
- Kozhoukharov D (1968) Precambrian. Proterozoic complex. In: *Stratigraphy of Bulgaria*, Science, Sofia, 5–62 (in Bulgarian)
- Kozhoukharov D (1984) Lithostratigraphy of Precambrian metamorphic rocks from Rhodope supergroup in the Central Rhodopes. *Geologica Balcanica*, **14**, 1, 43–88 (in Russian)
- Kozhoukharov D, Marinova R, Katskov N (1989) Geological map of Bulgaria in 1:100000 scale, map sheet Smolyan
- Kozhoukharova E, Kozhukharov D (1980) Problems of Precambrian in Bulgaria. *Geologica Balcanica*, **10**, 1, 75–94 (in Russian)
- Kruhl JH (1996) Prism- and basal-plane parallel subgrain boundaries in quartz: a microstructural geothermobarometer. *Journal of Metamorphic Geology*, **14**, 581–589
- Leake BE, Woolley AR, Arps CES, Birch WD, Gilbert MC, Grice JD, Hawthorne FC, Kato A, Kisch HJ, Krivovichev VG, Linthout K, Laird J, Mandarino JA, Maresch WV, Nickel EH, Rock NMS, Schumacher JC, Smith DC, Stephenson NCN, Ungaretti L, Whittaker EJW, Youzhi G (1997) Nomenclature of amphiboles: report of the Subcommittee on amphiboles of the International Mineralogical Association, Commission on new minerals and mineral names. *Canadian Mineralogist*, **35**, 219–246
- Leake BE, Woolley AR, Birch WD, Burke EAJ, Ferraris G, Grice JD, Hawthorne FC, Kisch HJ, Krivovichev VG, Schumacher JC, Stephenson NCN, Whittaker EJW (2003) Nomenclature of amphiboles: additions and revisions to the International Mineralogical Association's 1997 recommendations. *Canadian Mineralogist*, **41**, 1355–1362
- Liati A (2005) Identification of repeated Alpine (ultra) high-pressure metamorphic events by U–Pb SHRIMP geochronology and REE geochemistry of zircon: the Rhodope zone of Northern Greece. *Contributions to Mineralogy and Petrology*, **150**, 608–630
- Machev Ph, Kolcheva K (2008) Eclogites from Arda tectonic unit — mineralogy and evidence for short-leaved granulite facies overprint. *Proceedings of National Conference GEOSCIENCES 2008*, 49–50
- Mehnert KR, Busch W, Schneider G (1973) Initial melting at grain boundaries of quartz and feldspar in gneisses and granulites. *Neues Jahrbuch für Mineralogie*, **4**, 165–183
- Naydenov K, Nikolov D, Voynova E, Sarov S (2005) Preliminary data on a ductile strike-slip shear zone in Arda river valley (Central Rhodopes) – the Smilyan strike-slip. *Review of the Bulgarian Geological Society*, 80-th Anniversary, 43–45 (in Bulgarian)
- Ovtcharova M, Cherneva Z, von Quadt A, Peycheva I (2002) Migmatitic geochronology and geochemistry – a key to understanding the exhumation of the Madan dome (Bulgaria). *12 Annual Goldschmidt Conference Abstracts, Davos, Switzerland*, A573
- Ovtcharova M, von Quadt A, Cherneva Z, Peycheva I, Heinrich CA, Kaiser-Rohrmeier M, Neubauer F, Frank M (2003) Isotope and Geochronological Study on Magmatism and Migmatization in the Central Rhodopean Core Complex, Bulgaria. Programme and Abstracts, *Final GEODE-ABCD Workshop, Austria*, 42
- Ovcharova M (2004) Petrology, geochronology and isotope studies on metagranitoids from the eastern part of the Madan-Davidkovo Dome. *Unpublished PhD Thesis. Sofia University*, 235 p. (in Bulgarian)
- Papanikolaou D, Panagopoulos A (1981) On the structural style of southern Rhodope, Greece. *Geologica Balcanica*, **11**, 3, 13–22

- Passchier CV, Trouw RAJ (1996) *Microtectonics*. Berlin: Springer-Verlag, Germany, 289 p.
- Perchuk LL, Lavrentieva IV (1983) Experimental investigation of exchange equilibria in the system cordierite-garnet-biotite; 3. In: Kinetics and equilibrium in mineral reactions. Saxena-Surendra-K (editor) In the collection: *Advances in physical geochemistry*. 199-239 p.
- Peytcheva I, Salnikova E, Kostitsyn Y, Ovcharova M, Sarov S (2000) Metagranites from the Madan-davidkovo dome, central Rhodopes: U-Pb and Rb-Sr protholite and metamorphism dating. – In: Geodynamics and Ore Deposits Evolution of the Alpine-Carpathian-Dinaride Province. *ABCD-GEODE Workshop, Borovets, Bulgaria, Abstracts*, 66
- Peytcheva I, von Quadt A, Ovtcharova M, Handler R, Neubauer F, Salnikova E, Kostitsyn Y, Sarov S, Kolcheva K (2004) Metagranitoids from the eastern part of the Central Rhodopean Dome (Bulgaria): U-Pb, Rb-Sr and $^{40}\text{Ar}/^{39}\text{Ar}$ timing of emplacement and exhumation and isotopic-geochemical features. *Mineralogy and Petrology*, **82**, 1-31
- Pristavova S (1995) Evolution of metamorphism in the Precambrian rocks from Arda region. *PhD summary*, 37 p. (in Bulgarian)
- Raeva E (2009) Geochemistry of granites and metagranites along the Arda river upper valley, Central Rhodopes, Bulgaria. *Unpublished PhD Thesis. Sofia University*, 216 p. (in Bulgarian)
- Raeva E, Cherneva Z, Georgieva M (2008a) Geochemistry of the Madan unit gneisses from the Arda-river valley, Central Rhodopes, Bulgaria. *Jubilee collection of Sofia University "St. Kliment Ohridski"*, 60 years speciality *Geology*, 39-44
- Raeva E, Peytcheva I, Ovtcharova M, Cherneva Z (2008b) U-Pb zircon dating of granites and orthogneisses from the Madan unit in the Arda river valley, Central Rhodopes, Bulgaria. *Proceedings of National Conference GEOSCIENCES 2008*, 37-38
- Sarov S, Cherneva Z, Kolcheva K, Voinova E, Gerdgikov Y (2004) Lithotectonic subdivision of the metamorphic rocks from the eastern parts of the Central Rhodope extension structure. *Review of the Bulgarian Geological Society*, **65**, 1-3, 1-13 (in Bulgarian)
- Sarov S, Moskovski S, Zelezarski T, Georgieva I, Voynova E, Naydenov K, Nikolov D, Petrov N, Markov N (2005) Results from the geological investigations on geological task: "Drawing of National Geological Map of Bulgaria – Geological re-mapping in 1:50 000 scale of the Central Rhodopes in the region of cities Smolyan, Chepelare, Asenovgrad and Perushtitsa", *Geofund KG* (in Bulgarian)
- Sawyer EW (1999) Criteria for the recognition of partial melting. *Physics and Chemistry of the Earth*, (A), **24**, 269-279
- Schmidt MW (1992) Amphibole composition in tonalite as a function of pressure: an experimental calibration of the Al in hornblend barometer. *Contributions to Mineralogy and Petrology*, **110**, 304-310
- Schmidt S, Nagel TJ, Froitzheim N (2009) A new location with micro-diamond-bearing metamorphic rocks south of Sidironero (SW Rhodopes, Greece). *Alpine Workshop 2009 Conference Abstracts, Cogne, Italy*
- Siivola J, Schmid R (2007) A systematic nomenclature for metamorphic rocks: 12. List of mineral abbreviations. Recommendations by the IUGS Subcommission on the Systematics of Metamorphic Rocks. Recommendations, web version of 01.02.2007. www.bgs.ac.uk/scmr/home.html, 14 p
- Srivastava P, Mitra G (1996) Deformation mechanisms and inverted thermal profile in the North Almora Thrust mylonite zone, Kumaon Lesser Himalaya, India. *Journal of Structural Geology*, **18**, 27-39
- Stewart DB, Wright TL (1974) Al-Si order and symmetry of natural alkali feldspar and the relationship of strained cell parameters to bulk composition. *Bulletin Society for Mineralogy and Crystallography*, **97**, 356-377
- Stipp M, Stünitz H, Heilbronner R, Schmid S (2002) The eastern Tonale fault zone: a "natural laboratory" for crystal plastic deformation of quartz over a temperature range from 250 to 700°C. *Journal of Structural Geology*, **24**, 1861-1884
- Thompson AB (1976) Mineral reactions in pelitic rocks. II. Calculation of some P-T-X (Fe-Mg) phase reactions. *American Journal of Science*, **276**, 425-454
- Tullis J (1983) Deformation of feldspars. In: Ribbe PH (Editor), *Feldspar mineralogy*. (Reviews in Mineralogy, Vol. 2). *Mineralogical Society of America, 2nd Ed. Washington. DC*, 297-323 p.
- Vergilov V (1960) Petrological study of the crystalline schists from northern slope of the Central and Western Rhodopes. *News of the Geological Institute, BAS*, **9**, 223-269 (in Bulgarian)

- Vergilov V, Kozhuharov D, Boyanov I, Mavrudchiev B, Kozhuharova E (1963) Notes on Precamrian metamorphic complexes in Rhodope massif. *News of the Geological Institute, BAS*, **12**, 187-211 (in Bulgarian)
- Vernon RH (1975) Deformation and recrystallization of a plagioclase grain. *American Mineralogist*, **60**, 884-888
- Vernon RH (1977) Relationships between microstructures and metamorphic assemblages. *Tectonophysics*, **39**, 439-452
- Vernon RH, Clarke GL (2008) Principles of metamorphic petrology. *Cambridge University Press, New York*, XIII, 446 p.
- Vielzeuf D, Baronnet A, Perchuk AL, Laporte D, Baker MB (2007) Calcium diffusivity in alumino-silicate garnets : an experimental and ATEM study. *Contributions to Mineralogy and Petrology*, **154**, 2, 153-170
- Voll G (1976) Recrystallization of quartz, biotite and feldspars from Erstfeld to the Leventina Nappe, Swiss Alps, and its geological significance. *Schweizerische Mineralogische und Petrographische Mitteilungen*, **56**, 641-647
- von Quadt A, Sarov S, Peytcheva I, Voynova E, Petrov N, Nedkova K, Naydenov K (2006) Metamorphic rocks from northern parts of Central Rhodopes - conventional and in situ U-Pb zircon dating, isotope tracing and correlations. *Proceedings Joint Conference of Bulgarian Geophysical and Geological Societies "Geosciences 2006"*, 225-228
- Wen S, Nekvasil H (1994) SOLVCALC: An interactive graphics program package for calculating the ternary feldspar solvus and for two-feldspar geothermometry. *Computers & Geosciences*, **20**, 6, 1025-1040
- Wright TL (1968) X-ray and optical study of alkali feldspar. II. An X-ray method for determining the composition and structural state from measurement of 2 values for three reflections. *American Mineralogist*, **53**, 1/2, 88-104
- Wu Ch, Zhang J, Ren L (2004) Empirical garnet-biotite-plagioclase-quartz (GBPQ) geobarometry in medium to high-grade metapelites. *Journal of Petrology*, **45**, 9, 1907-1921

Accepted September 25, 2009

Appendix: Table 1. Selected plagioclase analyses: (r) rim; (c) core; (s) small grains; (l) large grains; (g) near garnet; (i) inclusion

Points	SiO ₂	TiO ₂	Al ₂ O ₃	Fe ₂ O ₃	CaO	Na ₂ O	K ₂ O	BaO	Total	X Ab	X An	X Or	X Cn	Al/Si
Orthogneiss E159A														
2 r	61.43	0.00	24.31	0.14	6.07	7.65	0.28	0.12	100.00	0.682	0.299	0.016	0.002	
9 c	61.58	0.00	24.41	0.00	5.93	7.45	0.38	0.14	99.89	0.677	0.298	0.023	0.003	
Orthogneiss E166														
2 r	60.89	0.00	25.46	0.15	5.73	7.42	0.32	0.00	99.98	0.687	0.293	0.020	0.000	
3 c	60.22	0.02	25.87	0.07	6.11	7.15	0.36	0.02	99.82	0.665	0.313	0.022	0.000	
6 c	61.34	0.05	25.18	0.13	5.36	7.55	0.39	0.00	100.00	0.701	0.275	0.024	0.000	
9 c	60.09	0.00	26.15	0.00	6.31	7.10	0.35	0.00	100.00	0.656	0.323	0.021	0.000	
Orthogneiss E171														
3 r	60.29	0.00	25.09	0.13	6.58	7.49	0.29	0.06	99.91	0.661	0.321	0.017	0.001	
4 c	60.95	0.06	24.66	0.11	6.42	7.37	0.34	0.09	99.99	0.661	0.318	0.020	0.002	
14 s	60.99	0.00	24.58	0.09	6.35	7.51	0.29	0.11	99.92	0.669	0.312	0.017	0.002	
21 s	60.65	0.04	24.89	0.04	6.56	7.13	0.36	0.09	99.76	0.648	0.329	0.022	0.002	
Orthogneiss E173														
2 r	61.83	0.00	24.41	0.07	5.76	7.41	0.33	0.02	99.83	0.685	0.294	0.020	0.000	
3 r	59.53	0.00	25.78	0.08	7.29	6.78	0.15	0.00	99.60	0.622	0.370	0.009	0.000	
9 r	62.89	0.05	23.40	0.05	4.86	8.14	0.32	0.00	99.72	0.738	0.243	0.019	0.000	
Paragneiss E168A														
10 l	59.67	0.06	24.89	0.08	6.16	8.17	0.44	0.00	99.55	0.689	0.287	0.024	0.000	
1 l	60.41	0.00	24.65	0.16	5.85	8.32	0.45	0.21	100.05	0.700	0.272	0.025	0.004	
5 s-g	58.46	0.00	26.63	0.17	7.58	7.22	0.15	0.00	100.21	0.627	0.364	0.009	0.000	
7 s	59.35	0.00	25.81	0.26	6.79	7.68	0.24	0.00	100.13	0.663	0.324	0.014	0.000	
9 s	59.12	0.00	25.09	0.09	6.62	8.29	0.22	0.00	99.43	0.686	0.303	0.012	0.000	
5' l-g	58.67	0.00	26.07	0.21	7.70	7.14	0.08	0.00	99.87	0.624	0.372	0.005	0.000	
4 l-g	58.51	0.27	25.94	0.18	7.84	7.02	0.31	0.00	100.07	0.607	0.375	0.018	0.000	
1' l-g	59.23	0.00	25.62	0.12	7.24	7.04	0.45	0.29	99.99	0.618	0.351	0.026	0.005	
13 l-g	58.13	0.03	26.48	0.23	8.11	6.95	0.07	0.00	100.00	0.606	0.390	0.004	0.000	
14 l-g	58.54	0.08	26.25	0.03	7.32	7.29	0.33	0.16	100.00	0.629	0.349	0.019	0.003	
Amphibolite E209														
2 r	58.98	0.00	25.69	0.09	7.69	7.49	0.09	0.10	100.13	0.634	0.360	0.005	0.002	0.514
8 r	58.56	0.00	26.11	0.36	7.38	7.50	0.10	0.16	100.17	0.642	0.349	0.006	0.003	0.526
1 c	59.22	0.00	25.91	0.11	7.21	7.49	0.20	0.45	100.59	0.640	0.341	0.011	0.008	0.516
9 c	59.39	0.00	26.30	0.00	7.63	7.09	0.12	0.29	100.82	0.620	0.368	0.007	0.005	0.522
10 i	59.53	0.08	25.82	0.04	7.52	7.37	0.09	0.00	100.45	0.636	0.359	0.005	0.000	0.511
13 i	58.70	0.13	26.13	0.18	7.64	6.96	0.13	0.14	100.01	0.616	0.374	0.008	0.003	0.525

Appendix: Table 2. Selected K-feldspar analyses: (c) core; (r) rim; (s) small grains

Points	SiO ₂	TiO ₂	Al ₂ O ₃	Fe ₂ O ₃	CaO	Na ₂ O	K ₂ O	BaO	Total	X Ab	X An	X Or	X Cn
Orthogneiss E159A													
12 c	65.20	0.00	18.17	0.00	0.15	1.37	14.36	0.58	99.83	0.125	0.008	0.857	0.011
13 r	65.10	0.10	18.19	0.04	0.09	1.21	14.65	0.50	99.89	0.110	0.005	0.876	0.009
16 r	65.22	0.04	18.21	0.01	0.00	0.89	14.87	0.66	99.90	0.082	0.000	0.905	0.012
11 s	65.01	0.00	18.10	0.01	0.09	0.84	15.40	0.54	100.00	0.075	0.004	0.910	0.010
Orthogneiss E166													
21 s	64.23	0.00	18.96	0.01	0.05	0.76	15.30	0.54	99.86	0.069	0.003	0.918	0.010
22 s	64.24	0.00	19.21	0.00	0.10	0.75	15.16	0.47	99.93	0.069	0.005	0.917	0.009
Orthogneiss E171													
1 s	65.10	0.04	18.45	0.05	0.07	1.03	14.91	0.35	100.00	0.094	0.004	0.896	0.007
2 s	64.82	0.00	18.06	0.06	0.08	0.80	15.57	0.57	99.97	0.072	0.004	0.914	0.010
9 s	65.02	0.03	18.21	0.04	0.09	1.13	14.95	0.35	99.83	0.102	0.005	0.887	0.006
15 s	64.73	0.13	18.31	0.10	0.11	0.98	15.12	0.44	99.91	0.089	0.005	0.898	0.008
Orthogneiss E173													
1 s	65.16	0.01	18.49	0.05	0.11	0.59	15.04	1.12	100.57	0.055	0.005	0.918	0.021
8 s	64.18	0.00	18.64	0.04	0.04	0.86	14.99	1.16	99.92	0.078	0.002	0.898	0.021
Paragneiss E163													
24 s	64.33	0.00	19.30	0.00	0.05	0.98	14.37	0.93	99.96	0.003	0.092	0.889	0.017
27 r	64.01	0.00	19.47	0.01	0.02	0.92	14.66	0.73	99.83	0.001	0.086	0.899	0.014
28 c	63.94	0.00	19.62	0.12	0.09	1.14	14.18	0.86	99.95	0.005	0.107	0.872	0.016
Paragneiss E168A													
6 r	65.51	0.00	18.33	0.08	0.00	1.46	14.32	0.30	100.00	0.134	0.000	0.861	0.005

Appendix: Table 3. Selected biotite analyses from paragneisses, orthogneisses and amphibolites: (l) large; (s) small

Rock type	Paragneiss										
Sample	E168A									E163	
Point	111	231	16 s	28 s	351	81	91	31	121	151	181
SiO ₂	37.44	34.86	36.22	36.39	36.28	36.87	36.99	36.57	37.13	35.46	36.55
TiO ₂	1.79	1.71	1.88	2.12	1.74	3.00	3.25	3.09	2.84	3.11	3.08
Al ₂ O ₃	16.56	16.55	16.79	16.69	16.96	16.49	16.05	16.17	16.44	19.07	19.39
FeO	21.44	22.74	21.16	20.74	20.92	21.44	21.89	21.00	21.88	18.12	18.37
MnO	0.36	0.46	0.37	0.70	0.52	0.56	0.58	0.50	0.87	0.32	0.29
MgO	10.20	9.48	10.68	9.41	10.08	8.73	8.36	9.10	8.98	9.40	9.83
CaO	0.00	0.00	0.00	0.00	0.00	0.00	0.00	0.00	0.00	0.10	0.01
Na ₂ O	0.00	0.00	0.00	0.00	0.00	0.00	0.00	0.49	0.00	0.10	0.10
K ₂ O	8.84	10.17	9.32	9.98	9.65	9.59	9.83	9.80	9.27	9.63	9.73
Total	96.63	95.97	96.42	96.03	96.15	96.68	96.95	96.72	97.41	95.31	97.36
<i>apfu at 22 O atoms</i>											
Si	5.64	5.42	5.50	5.57	5.53	5.60	5.62	5.56	5.60	5.38	5.41
Ti	0.20	0.20	0.21	0.24	0.20	0.34	0.37	0.35	0.32	0.35	0.34
Al ^{IV}	2.36	2.58	2.50	2.43	2.47	2.40	2.38	2.44	2.40	2.62	2.59
Al ^{VI}	0.59	0.45	0.51	0.58	0.58	0.55	0.50	0.46	0.52	0.79	0.79
Cr	0.00	0.00	0.00	0.00	0.00	0.00	0.00	0.00	0.00	0.00	0.00
Fe ⁺³	0.00	0.00	0.00	0.00	0.00	0.00	0.00	0.00	0.00	0.00	0.00
Fe ⁺²	2.70	2.96	2.69	2.65	2.67	2.72	2.78	2.67	2.76	2.30	2.27
Mn	0.05	0.06	0.05	0.09	0.07	0.07	0.07	0.06	0.11	0.04	0.04
Mg	2.29	2.20	2.42	2.15	2.29	1.97	1.89	2.06	2.02	2.12	2.17
Ca	0.00	0.00	0.00	0.00	0.00	0.00	0.00	0.00	0.00	0.02	0.00
Na	0.00	0.00	0.00	0.00	0.00	0.00	0.00	0.14	0.00	0.03	0.03
K	1.70	2.02	1.81	1.95	1.88	1.86	1.91	1.90	1.78	1.86	1.84
Totals	15.53	15.88	15.68	15.66	15.68	15.51	15.52	15.66	15.51	15.51	15.49
Fe ²⁺ /(Fe ²⁺ + Mg)	0.54	0.57	0.53	0.55	0.54	0.58	0.60	0.56	0.58	0.52	0.51

Table 3. (continuation)

Rock type	Orthogneiss									Amphibolite	
Sample	E159A			E166		E171				E209	
Point	8	17	18	14	15	5	7	8	11	27	28
SiO ₂	35.54	35.51	36.26	36.69	36.00	35.86	36.02	36.16	36.16	35.57	36.11
TiO ₂	4.48	3.77	3.46	3.47	2.99	3.57	3.47	2.86	3.18	1.65	1.71
Al ₂ O ₃	15.89	16.68	16.32	17.17	16.59	15.19	14.99	15.55	15.33	19.99	20.12
FeO	20.98	20.30	21.47	20.37	19.91	20.55	19.59	20.44	21.09	16.48	15.47
MnO	0.57	0.56	0.53	0.43	0.44	0.34	0.38	0.32	0.29	0.08	0.11
MgO	7.89	8.03	7.96	9.79	10.04	8.96	9.24	9.71	9.71	12.18	13.03
CaO	0.02	0.07	0.00	0.01	0.04	0.03	0.11	0.05	0.00	0.00	0.00
Na ₂ O	0.06	0.13	0.07	0.06	0.10	0.03	0.04	0.09	0.04	0.00	0.00
K ₂ O	9.69	9.60	9.63	9.95	9.67	9.67	9.62	9.56	9.69	9.25	9.27
Total	95.12	94.63	95.69	97.94	95.76	94.21	93.46	94.73	95.48	95.20	95.82
<i>apfu at 22 O atoms</i>											
Si	5.51	5.50	5.58	5.48	5.50	5.59	5.64	5.59	5.57	5.33	5.34
Ti	0.52	0.44	0.40	0.39	0.34	0.42	0.41	0.33	0.37	0.19	0.19
Al ^{IV}	2.49	2.50	2.42	2.52	2.50	2.41	2.36	2.41	2.43	2.67	2.66
Al ^{VI}	0.41	0.55	0.53	0.50	0.48	0.39	0.41	0.43	0.36	0.86	0.85
Cr	0.00	0.00	0.00	0.00	0.00	0.00	0.00	0.00	0.00	0.00	0.00
Fe ⁺³	0.00	0.00	0.00	0.00	0.00	0.00	0.00	0.00	0.00	0.00	0.00
Fe ⁺²	2.72	2.63	2.76	2.54	2.54	2.68	2.56	2.65	2.72	2.06	1.91
Mn	0.07	0.07	0.07	0.05	0.06	0.05	0.05	0.04	0.04	0.01	0.01
Mg	1.82	1.86	1.82	2.18	2.28	2.08	2.16	2.24	2.23	2.72	2.87
Ca	0.00	0.01	0.00	0.00	0.01	0.00	0.02	0.01	0.00	0.00	0.00
Na	0.02	0.04	0.02	0.02	0.03	0.01	0.01	0.03	0.01	0.00	0.00
K	1.91	1.90	1.89	1.89	1.88	1.92	1.92	1.89	1.91	1.77	1.75
Totals	15.49	15.50	15.52	15.58	15.62	15.56	15.54	15.61	15.63	15.61	15.59
Fe ²⁺ /(Fe ²⁺ + Mg)	0.60	0.59	0.60	0.54	0.53	0.56	0.54	0.54	0.55	0.43	0.40

Appendix: Table 4. Selected garnet analyses from paragneiss sample E1684: (c) core; (r) rim; (b) near biotite; (p) near plagioclase

Point	12r-b	13r-p	14c	22r	20c	17r	18c	27r	29c	34r-b	36r-p	33c	6r	7c	2c	11r	10c
SiO ₂	39.06	38.83	38.05	35.59	37.35	38.18	38.08	37.94	38.49	37.84	36.87	37.11	36.98	37.03	36.93	37.29	37.45
TiO ₂	0.00	0.00	0.00	0.00	0.00	0.00	0.00	0.00	0.00	0.00	0.00	0.00	0.04	0.05	0.15	0.31	0.00
Al ₂ O ₃	21.06	20.95	21.02	18.96	21.24	21.23	21.06	20.87	20.98	21.34	21.08	20.43	20.88	21.05	20.44	20.63	20.98
FeO	23.20	24.08	27.73	29.21	27.50	24.14	27.35	24.93	24.79	24.90	26.93	28.69	23.44	28.42	27.66	25.46	27.66
MnO	6.18	5.94	6.41	7.22	7.33	5.95	6.00	6.90	6.58	6.57	6.71	6.69	6.93	7.20	7.79	7.27	7.14
MgO	1.91	2.79	2.88	2.07	3.04	2.70	2.86	2.56	1.74	2.50	3.14	2.93	1.46	2.61	2.16	1.61	2.41
CaO	8.64	7.24	3.64	6.41	3.03	7.84	4.35	6.05	7.74	6.74	5.15	3.54	8.13	3.54	3.53	6.75	3.74
Total	100.05	99.83	99.73	99.46	99.49	100.04	99.70	99.25	100.32	99.89	99.88	99.43	97.87	100.00	98.82	99.01	99.38
<i>apfu</i> at 12 O atoms																	
Si	3.08	3.07	3.04	2.94	3.00	3.02	3.04	3.04	3.04	3.05	3.01	2.96	3.00	3.01	2.98	3.01	3.02
Ti	0.00	0.00	0.00	0.00	0.00	0.00	0.00	0.00	0.00	0.00	0.00	0.00	0.00	0.01	0.02	0.00	0.00
Al	1.96	1.95	1.98	2.01	1.98	1.98	1.97	1.97	1.96	2.00	2.00	1.95	2.01	2.00	1.96	1.97	2.00
F _{Fe²⁺}	1.53	1.59	1.85	2.02	1.85	1.60	1.83	1.67	1.65	1.66	1.81	1.94	1.60	1.91	1.89	1.73	1.87
Mn	0.41	0.40	0.43	0.51	0.50	0.40	0.41	0.47	0.47	0.44	0.44	0.46	0.46	0.48	0.49	0.54	0.50
Mg	0.23	0.33	0.34	0.26	0.36	0.32	0.34	0.31	0.21	0.30	0.38	0.35	0.18	0.31	0.26	0.19	0.29
Ca	0.73	0.61	0.31	0.57	0.26	0.67	0.37	0.52	0.66	0.58	0.44	0.31	0.71	0.31	0.59	0.32	0.32
Total	7.94	7.95	7.97	8.14	7.99	7.99	7.97	7.98	7.97	7.99	8.04	8.02	7.98	8.01	7.99	7.98	7.98
X Alm	0.53	0.54	0.63	0.60	0.62	0.54	0.62	0.56	0.56	0.56	0.59	0.63	0.54	0.63	0.63	0.57	0.63
X Ppp	0.08	0.11	0.12	0.08	0.12	0.11	0.12	0.10	0.07	0.10	0.12	0.12	0.10	0.10	0.09	0.06	0.10
X Grs	0.25	0.21	0.11	0.17	0.09	0.22	0.13	0.18	0.22	0.19	0.14	0.10	0.24	0.10	0.10	0.20	0.11
X Sp	0.14	0.14	0.15	0.15	0.17	0.13	0.14	0.16	0.15	0.15	0.15	0.16	0.16	0.16	0.18	0.17	0.16
#Fe*	0.87	0.83	0.84	0.89	0.84	0.83	0.84	0.85	0.85	0.83	0.85	0.90	0.86	0.88	0.90	0.87	

* #Fe = Fe²⁺ / (Fe²⁺ + Mg)

Appendix: Table 5. Selected amphibole analyses from amphibolite sample E209: Fe^{3+} from 13-CNK, r - rim, c - core, i - inclusion

Points	3 r	7 r	4 c	6 c	5 i	11 i	12 i
SiO ₂	43.23	43.49	43.45	43.84	42.98	43.50	42.74
TiO ₂	0.75	0.97	1.15	1.01	0.93	1.20	1.10
Al ₂ O ₃	12.57	12.68	12.06	12.57	12.35	12.20	12.10
FeO	16.28	16.30	17.28	16.34	16.60	15.44	15.89
MnO	0.58	0.48	0.53	0.30	0.48	0.49	0.24
MgO	10.01	9.71	9.68	10.04	9.75	10.47	10.29
CaO	11.41	11.86	11.56	11.69	11.42	11.65	11.99
Na ₂ O	1.43	1.52	1.26	1.39	1.48	1.62	1.60
K ₂ O	0.73	0.73	0.48	0.65	0.60	0.71	0.56
Total	96.99	97.74	97.45	97.83	96.59	97.28	96.51
<i>apfu at 23 O atoms</i>							
Si	6.413	6.448	6.429	6.454	6.418	6.447	6.412
Al [IV]	1.587	1.552	1.571	1.546	1.582	1.553	1.588
<i>T</i>	8	8	8	8	8	8	8
Al [VI]	0.610	0.664	0.532	0.635	0.592	0.578	0.551
Ti	0.084	0.108	0.128	0.112	0.104	0.134	0.124
Cr	0.000	0.000	0.000	0.000	0.000	0.000	0.000
Fe ³⁺	0.633	0.328	0.666	0.480	0.585	0.408	0.363
Fe ²⁺	1.386	1.693	1.472	1.532	1.488	1.505	1.630
Mn	0.073	0.060	0.066	0.037	0.061	0.062	0.030
Mg	2.214	2.146	2.135	2.204	2.171	2.313	2.301
<i>C</i>	5	5	5	5	5	5	5
Ca	1.813	1.884	1.833	1.844	1.827	1.850	1.927
Na	0.187	0.116	0.167	0.156	0.173	0.150	0.073
<i>B</i>	2	2	2	2	2	2	2
Na	0.225	0.321	0.194	0.241	0.255	0.315	0.392
K	0.138	0.138	0.091	0.122	0.114	0.134	0.107
<i>A</i>	0.363	0.459	0.285	0.363	0.370	0.449	0.499
T=13	13.18	13.09	13.19	13.14	13.17	13.12	13.10
Mg/(Mg+Fe ²⁺)	0.61	0.56	0.59	0.59	0.59	0.61	0.59
Al/Si	0.343	0.344	0.327	0.338	0.327	0.331	0.334

